A FRAMEWORK FOR OPTIMIZING PROCESS PARAMETERS IN POWDER BED FUSION (PBF) PROCESS USING ARTIFICIAL NEURAL NETWORK (ANN)

A Thesis

Submitted to the Faculty

of

Purdue University

by

Mallikharjun Marrey

In Partial Fulfillment of the

Requirements for the Degree

of

Master of Science in Mechanical Engineering

August 2019

Purdue University

Indianapolis, Indiana

THE PURDUE UNIVERSITY GRADUATE SCHOOL
STATEMENT OF COMMITTEE APPROVAL

Dr. Hazim El-Mounayri, Chair

    Department of Mechanical and Energy Engineering

Dr. Andres Tovar

    Department of Mechanical and Energy Engineering

Dr. Jing Zhang

    Department of Mechanical and Energy Engineering

Approved by:

    Dr. Sohel Anwar

        Chair of the Graduate Program

Dedicated to Mom and Dad.

ACKNOWLEDGMENTS

I would like to express my sincere gratitude to my adviser, Dr. Hazim El-Mounayri, for his constant support and guidance throughout the thesis work. I express my gratitude towards my committee members, Dr. Andres Tovar and Dr. Jing Zhang for their valuable suggestions. I would like to thank Dr. Eric J. Faierson from Quad City Manufacturing Laboratory for printing the samples and making this work alive. I would also like to thank Michael Golub and Daniel Eugene Minner for their invaluable help during the testing phase.

I would like to express my deepest appreciation to Ehsan Malekipour, who guided me continually through countless nights and for his invaluable help during the publications. I will always be grateful to you.

Finally, I want to thank my parents and my girlfriend Jaswitha for believing in me and being there through thick and thin.

TABLE OF CONTENTS

LIST OF TABLES

LIST OF FIGURES

SYMBOLS

T_m	Melting temperature
T_0	Room temperature
q	heat per unit volume
c	Specific heat capacity
l_f	Latent heat of fusion
ρ	Density
η	Efficiency coefficient
η^*	Additional efficiency coefficient
R_{Powder}	Reflectivity of the powder feedstock
k_{rel}	Relative thermal conductivity of powder feedstock
n	Number of measurements
Y_i	Observed performance characteristic value
s	Standard deviation of responses
R_a	Surface roughness
L	Scan length
Y(x)	Profile of the curve
0	Predicted output
y	actual output

ABBREVIATIONS

AM	Additive manufacturing
PBF	Powder bed fusion
FF	Feed forward
BP	Back propogation
ANN	Artificial neural network
SLM	Selective laser melting
SLS	Selective laser sintering
DMLS	Direct metal laser sintering
LP	Laser power
SS	Scan speed
LT	Layer thickness
HS	Hatch space
BD	Beam diameter
SA	Sensitivity analysis
D	Densification
MS	Microstructure
FT	Fabrication time
MP	Mechanical properties
SR	Surface roughness
DA	Dimensional accuracy
VED	Volumetric energy density
DOE	Design of experiments
UTS	Ultimate tensile strength
ANOVA	Analysis of variance
LOF	Lack of fusion

SR	Surface roughness
FEM	Finite element method
FAST	Fourier amplitude sensitivity testing
WEDM	Wire electric discharge machining
SEM	Scanning electron microscope
BW	Black and white
OA	Orthogonal array
S/N	Signal to noise
ML	Machine learning
SVR	Support vector regression

ABSTRACT

Marrey, Mallikharjun. M.S.M.E., Purdue University, August 2019. A Framework for Optimizing Process Parameters in Powder Bed Fusion (PBF) Process Using Artificial Neural Network (ANN). Major Professor: Hazim El-Mounayri

Powder bed fusion (PBF) process is a metal additive manufacturing process, which can build parts with any complexity from a wide range of metallic materials. Research in the PBF process predominantly focuses on the impact of a few parameters on the ultimate properties of the printed part. The lack of a systematic approach to optimizing the process parameters for a better performance of given material results in a sub-optimal process limiting the potential of application. This process needs a comprehensive study of all the influential parameters and their impact on the mechanical and microstructural properties of a fabricated part. Furthermore, there is a need to develop a quantitative system for mapping the material properties and process parameters with the ultimate quality of the fabricated part to achieve improvement in the manufacturing cycle as well as the quality of the final part produced by the PBF process. To address the aforementioned challenges, this research proposes a framework to optimize the process for 316L stainless steel material. This framework characterizes the influence of process parameters on the microstructure and mechanical properties of the fabricated part using a series of experiments. These experiments study the significance of process parameters and their variance as well as study the microstructure and mechanical properties of fabricated parts by conducting tensile, impact, hardness, surface roughness, and densification tests, and ultimately obtain the optimum range of parameters. This would result in a more complete understanding of the correlation between process parameters and part quality. Furthermore, the data acquired from the experiments is employed to develop an intelligent parameter suggestion multi-layer feedforward (FF) back propagation (BP) artificial neural

network (ANN). This network estimates the fabrication time and suggests the parameter setting accordingly to the user/manufacturers desired charecteristics of the end-product. Further, research is in progress to evaluate the framework for assemblies and complex part designs and incorporate the results in the network for achieving process repeatability and consistency.

1. INTRODUCTION

1.1 Background

PBF process is the most widely used additive manufacturing technology for metal printing and functional parts [1]. A wide range of metallic powder can be used as raw material for this process [2]. As with any other additive technology, PBF fabricates parts directly from 3D CAD data (STL file) and eliminates the use of expensive tooling [3, 4]. STL file of the part is sliced into many layers with respect to the layer thickness and a laser beam sinters/melts each layer. Selective laser melting (SLM) and selective laser sintering (SLS) are the main two PBF processes. Unlike the SLM process where the powder is completely melted down to form a homogeneous part, the SLS process partially melts the material (sinters the powder) layer-by-layer at the molecular level [5]. The schematic diagram in Figure 1.1. shows the overall process of the PBF process [6]. The PBF machine typically consists of a supply station for the metal powder and a sintering/melting unit. A laser selectively sinters/melts the powder with respect to the layer geometry along a prescribed pattern. After sintering/melting of a layer, the powder-bed moves downward a distance equals to the thickness of a layer and a recoater arm or a roller transfers the material powder from the dispenser platform to the powder-bed. The same process continues until the fabrication of the last layer [7].

Due to the ability of the PBF process to produce homogeneous parts with high strength alloys and free-form geometry [4], it has found applications in various sectors such as aerospace, defense, automotive, medical, etc. [8-10] . The aerospace industry widely employs the PBF process because of advantages such as the ability to produce complex parts (optimized designs, which are difficult to manufacture with traditional techniques) and functional assemblies with a significant reduction in fabrication time
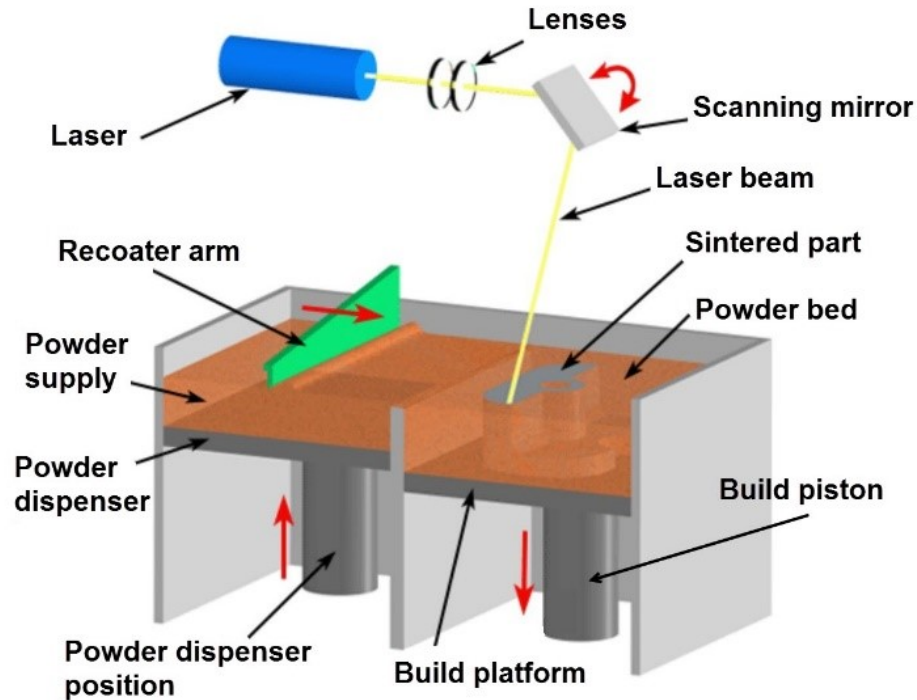
Figure 1.1. A schematic diagram of direct metal laser sintering (DMLS) process [6]

[8, 11]. A wide range of metals such as alloys of aluminum, cobalt chrome, copper-based, nickel-based, titanium, tool steels, and stainless steels are excellent materials for the aerospace industry, which are offering a significant cost and weight reduction [12, 13]. Automotive industry benefits from the PBF processes as well. In this industry, employment of topology optimization lets the designers to optimize and substitute the traditional design of Continuously Variable Transmission (CVT) [14, 15] with more weight effective complex geometry [10]. However, the new designs can be fabricated only by the PBF processes.

The PBF process has been employed in various industries however the potential is still limited due to some process drawbacks. To overcome these drawbacks, the research nowadays is concentrated on the impact of few parameters on the ultimate properties of printed parts [1, 5, 11, 16-21]. The ultimate objective is to develop a control system which maps manufacturing process, material properties, and the

ultimate quality of a fabricated part together. Such system will optimize the process parameters ultimately. Fulfilling this objective needs a comprehensive study on all the influential parameters with their significance on the mechanical and microstructural properties of a fabricated part. Furthermore, it needs to develop a quantitative system for mapping material property and process parameters to achieve improvement in the manufacturing cycle and quality control of the parts produced by the PBF process.

More than fifty parameters exist and have an influence on the ultimate quality of the product [22-24]. Scholars classify the process parameters into different groups [23-25]. In one approach, Malekipour et al. [24, 25] classified the parameters into three main categories. The first category is pre-processed parameters including environmental conditions such as an inert gas, oxygen level, ambient temperature, powder specifications, and machine capabilities/limitations. The second category is the controllable parameters, which include process parameters, namely, laser specifications and scan strategy, and few manufacturing specifications such as layer thickness. The last category includes the post-processed parameters, which quantify the ultimate quality of the fabricated part such as the yield strength, fatigue resistance, etc. [25]. Van Elsen [26] named some of the important parameters in each classification. He mentioned that the powder specifications and deposition include morphology, the surface roughness of the generated grains, particle size distribution, and the deposition system of powder on to the bed. The laser specifications include spot size, wavelength, peak power, mode of the laser, and laser pulse length. The process parameters include part placement, scan strategy, build direction, laser power, scan speed, scan strategy, layer thickness, preheating temperature, hatch distance, and energy density [26].

The aforementioned parameters influence the process and the fabrication cost [23]. For instance, the process utilizes Argon instead of Helium as an environment for Ti-6Al-4V because Helium is 3 to 4 times more expensive than Argon [26]. However, previous literature shows that among all the factors affecting the PBF process, few parameters, namely, laser power, scan speed, hatch spacing, layer thickness, beam

diameter, and preheating temperature have a tremendous impact on mechanical efficiency, economy, and ultimate quality of the entire PBF process [5, 9, 21, 27].

Although PBF technology has significantly developed and is employed in different industries, many challenges are still to be addressed. These challenges hinder the process repeatability, consistency, and stability of the process. Literature review (Chapter 2) shows that several research works have studied the influence of process parameters on quality for different materials and machines; however, it has proven very difficult to control all aspects of the process or evaluate the collective influence of all the parameters on the properties of a fabricated part. Scholars focused on identifying the influence of few process parameters, predominantly laser specifications, on the surface quality or selective mechanical properties of the printed part; limited research works studied the correlation between the parameters and the ultimate properties of the printed part. However, there is a lack of a consistent system considering/optimizing all the controllable parameters and mapping the process, material, and parameters onto the ultimate properties of the fabricated parts. Furthermore, Optimizing the machine setting by controlling the parameters is a prerequisite for a near flawless fabrication process.

The ultimate quality of a fabricated part predominantly depends upon controllable process parameters such as laser specifications and scan pattern. This work focuses on laser specifications namely, laser power, scan speed, and hatch space as well as layer thickness. The ultimate contribution of this work is to examine the effect of a set of parameters instead of the effect of their individual impact on the selected properties of a fabricated part. This will help to develop an offline control system, which lets vendors/customers choose the desirable process specifications such as mechanical properties versus fabrication time. The combination of this work with the recommended real-time control system in our research group [28] for controlling the thermal aspects of different printing patterns, will help to fill the existing gap for development of a comprehensive standardized control system. Such system will map all the contributing and controllable process parameters and material specifica-

tions onto the ultimate quality of fabricated parts. Furthermore, manufacturers can employ this system to ensure full compliance with the customer's demands.

This work proposes a two-phase framework (Figure 3.1) towards development of the first stage of the comprehensive control system, namely, optimization of set of process parameters. This framework which was recently published in [29], designed to pursue the objectives of this study. These objectives are first, to obtain a working range of volumetric energy density (VED) for the first phase using mathematical modelling and then conducting sensitivity analysis to identify which parameters affect the VED the most in the obtained range. Second, to determine the optimal range of the VED and the way that laser power and scan speed affect the microstructure, densification, and mechanical properties of a fabricated part. Third, to optimize laser power, scan speed, hatch spacing and beam diameter for fabricating a part within the VED with maximum density range obtained from phase-I for obtaining better ultimate quality; and finally, to develop an intelligent neural network for modeling the process by creating a correlation function between the process parameters and ultimate properties of the fabricated parts. This function helps in suggesting the optimized process parameters in order to fabricate parts in accordance with the users desired requirements, namely, mechanical properties, microstructure, fabrication time, dimensional accuracy, and surface roughness.

1.2 Motivation and problem statement

With the evolution of Industry 4.0, the application of advanced manufacturing technologies integrating with information management technologies for the creation of a smart manufacturing process plays an important role aiming to create smart factories by integrating the physical world and the cyber world to achieve economic competitiveness [30]. With the increasing necessity for mass customization, predictive modelling and for optimizing the part design to increase the mechanical properties and to reduce the weight of the parts, non-traditional manufacturing techniques like

AM has become key technologies for manufacturing. Figure 1.2 shows the schematic of smart factories with the implementation of industry 4.0. Exclusively, for manufacturing of metal components, metal additive manufacturing has proven the ability to manufacture free-form complex parts with better mechanical properties compared to traditional manufacturing. The increasing demand and interest in the application of AM in various industries such as aerospace, defense and biomedical, has led to significant research in standardizing the AM process. Although there are still some challenges which need to be addressed for making the process standardized. There are more than 50 process parameters that influence the ultimate part quality but among all those parameters, there are few controllable parameters which have a significant effect on the part quality [24, 25]. These parameters lead to the formation of in-process defects such as porosity and lack-of-fusion which in turn lead to substantial changes in the mechanical properties of the manufactured part [31]. Without controlling these parameters, the full potential of AM cannot be utilized. The understanding and recognition of the influence of process parameters on the process defects and the mechanical properties can leverage the predictive modelling and control of the process. This objective can be achieved by studying the process, material, defects and properties and mapping them together. Achieving this objective provides a complete understanding of the defects formation leading to predictive modelling of process parameters for obtaining the desired properties of the manufactured part and sequentially in standardizing the process. To date, scholars have been studying the effect of individual process parameters on the selected mechanical properties lacking in developing a system which considers a set of process parameters and studies their significance on microstructure, densification, surface roughness, fabrication time and mechanical properties. The major challenges/gaps existing in the current literature are lack of standardized system, inadequate information of effect of beam diameter on the quality properties, lacking consistency in results obtained by scholars for the same material, and most importantly lacking a predictive model for intelligent process parameter selection which can make the AM process smart. Chapter 2 provides

more insight into these challenges and gaps.This research work proposes a framework for studying the influence of process parameters on multiple properties of the manufactured part for optimizing the process parameters to obtain the ultimate quality of the part and develops an artificial neural network by training a back-propagating algorithm consequently in developing a predictive model of the process.
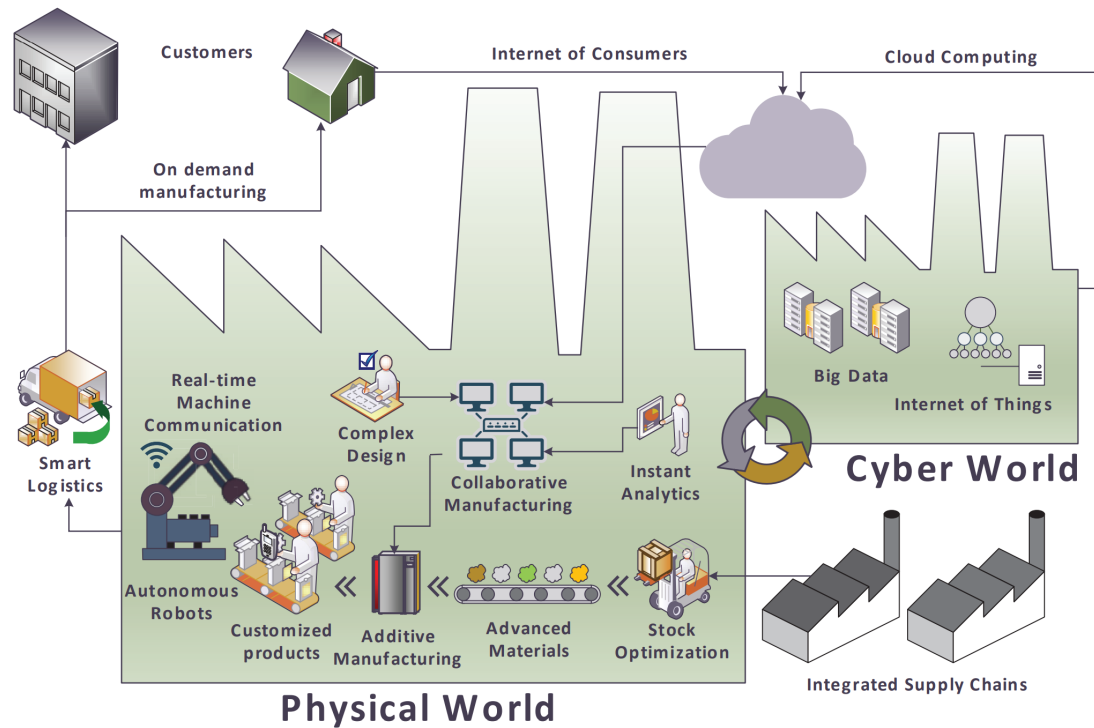
Figure 1.2. Schematic of general properties required in Industry 4.0 [30]

1.3   Research objectives

In the era of Industry 4.0, predictive modelling is a major notion for achieving smart manufacturing in the virtual world. For predictive modelling a process, a comprehensive interpretation of the process parameters, defects, and ultimate quality of the manufactured part is vital. Literature review (Chapter 2) shows that PBF

process lacks a practical system mapping process, material, defects and property and by governing the process parameters, defect generation and mechanical property anomalies can be avoided or significantly controlled. This research addresses the aforementioned challenges by achieving the following objectives.

- Proposing a framework for optimizing the PBF process.

- Understanding the influence of laser power (LS) and scan speed (SS) on the porosity and density and optimizing the LS, SS and volumetric energy density (VED) for achieving maximum density.

- Studying the influence of LP, SS, hatch spacing (HS), beam diameter (BD) on mechanical properties, surface roughness, dimensional accuracy and fabrication time and optimizing these parameters within the optimal range of energy density obtained from phase 1.

- Creating a mapping between process, parameters and ultimate properties of the manufactured part.

- Developing a feed forward back-propagating artificial neural network for predictive modelling of process parameter and build-time estimations.

1.4   Thesis outline

Chapter 1 introduces the PBF process, challenges, current gaps in the literature, potential areas to address with motivation and problem statement and the proposed framework. The research objectives address the mentioned challenges and achievements of this research work. In chapter 2, the significance of each process parameters on ultimate properties of the manufactured part is demonstrated in detail and the classification of common in-process defects and post-process defects with the approaches to avoid or significantly control is presented along with the detailed explanation about the existing challenges and gaps. To achieve the objectives of this work, chapter 3

proposes and implements the framework. In this chapter, the methodology of implementing the framework is explained in two phases. In phase 1, preliminary design of experiments (DOE) was conducted to optimize LP, SS and VED for achieving maximum density and uniform pore distribution. In phase 2, a comprehensive study on LP, SS, HS and BD and their influence on mechanical properties, surface roughness, dimensional accuracy, warpage and fabrication time are conducted. Analysis of variance (ANOVA) is conducted and chapter 4 presents the results obtained by implementing the framework. In chapter 4, the correlation between process parameters and quality properties is explained and optimum process parameters for obtaining ultimate part quality will be explicated. Chapter 5 presents the different types of algorithms and the development of ANN for predictive modelling incorporating the results from chapter 4. The testing of the developed ANN model and the efficiency with future expansion will be demonstrated in this chapter. Finally, chapter 5 provides the limitations, ongoing research, future work directions and conclusion.

2. LITERATURE REVIEW

With the increasing application of metal AM, quality control has become crucial for obtaining reliance on the adoption into mass production. As detailed in chapter 1, multiple parameters have a significant effect on the ultimate quality of the manufactured part and lead to defect formation if not controlled. In this chapter, we describe the significance of each parameter and their influence on defect generation along with a detailed description of the different defects generated during the PBF process is also provided. Also, the current gaps and challenges in the existing literature is elucidated.

2.1 Process parameters and their significance on ultimate properties in the metal additive manufacturing process

2.1.1 Introduction

PBF process has the ability to fabricate free-form complex parts with better ultimate properties. However, the desired quality of the part is inevitably affected by process parameter conditions, as a result leads to the formation of defects during the process. Malekipour et al. [25] classified the process parameters into three groups namely pre-processed parameters, controllable parameters and post-processed parameters. Figure 2.1 shows the classification of the parameters. From this classification, in this section, the influence of controllable parameters (LP, SS, HS, LT, build preheating) and pre-processed parameters (BD) and their effect of the defect formation is elucidated in detail.
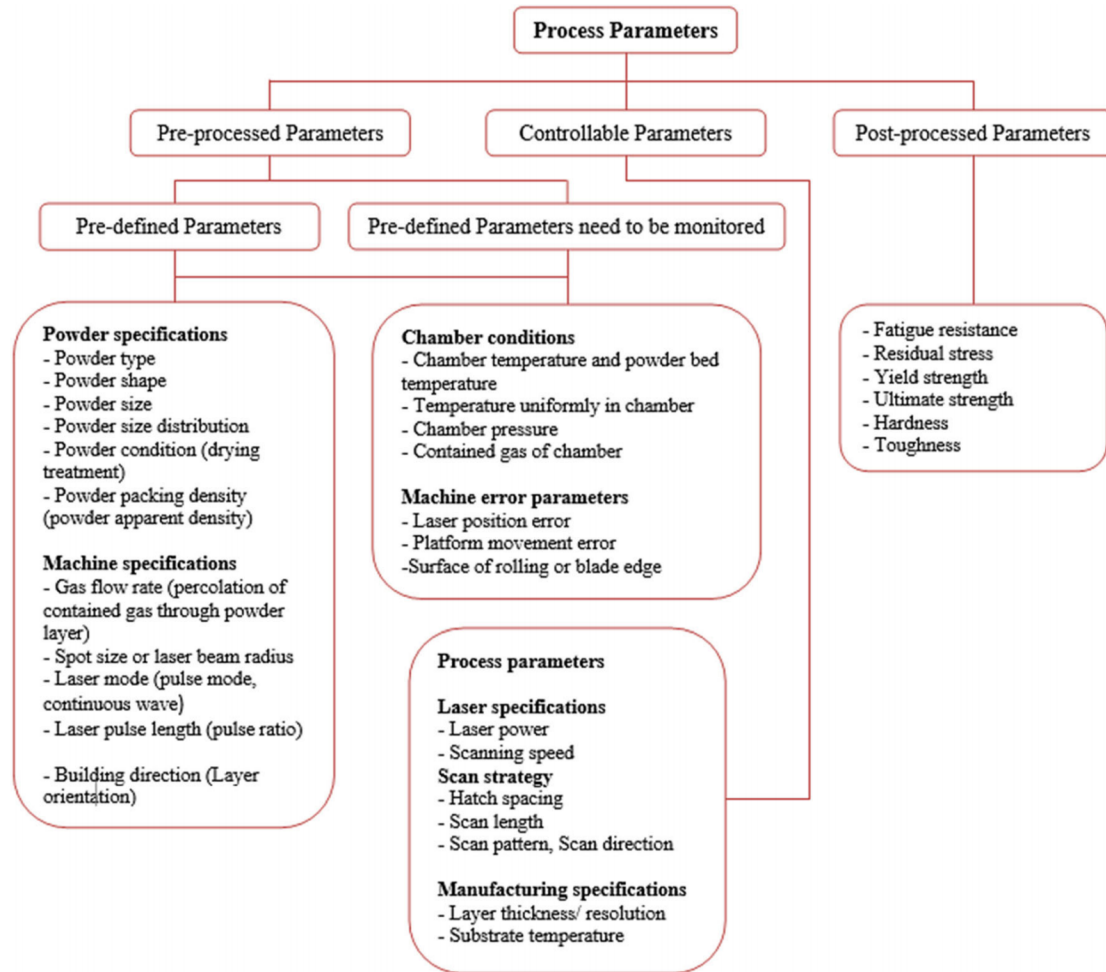
Figure 2.1. Classification of process parameters [22]

2.1.2 Laser power

The effect of laser power on the energy applied can significantly change the formation of the effective melt pool. LP is directly related to the energy applied. Wide range of LP setting options are available with the current PBF technology, but extensive work has been conducted in the range of 0W - 400W. With higher laser power, a high amount of energy is applied leading to vaporization of powder material trapping gas bubbles and formation of gas induced pores in the next layers.

With a decrease in LP, insufficient melting of powder occurs causing the formation of lack of fusion (LOF) pores. Also, with less energy application, the depth of laser penetration decreases causing insufficient melting of powder layer and fusing layers together forming cracks between layers [32]. There is an operating window where the LP values have to be adjusted to avoid defects such as balling, keyhole formation and LOF as shown in Figure 2.2. Scholars investigated the influence of different parameters related to volumetric energy density on density, geometrical characteristics and mechanical properties of single-track and complete builds and found that the most influential process parameter on the stated properties was LP followed by LT and SS [33, 34]. Also, build rate is directly related to the laser power input. With a laser power input of 380W, 72% increase in build rate is observed compared to the 100W laser power input [35] in PBF process. Ultimately, increasing LP up to a certain limit will result in bigger melt pools, a stronger bond between layers, lower porosity and better mechanical properties [36].
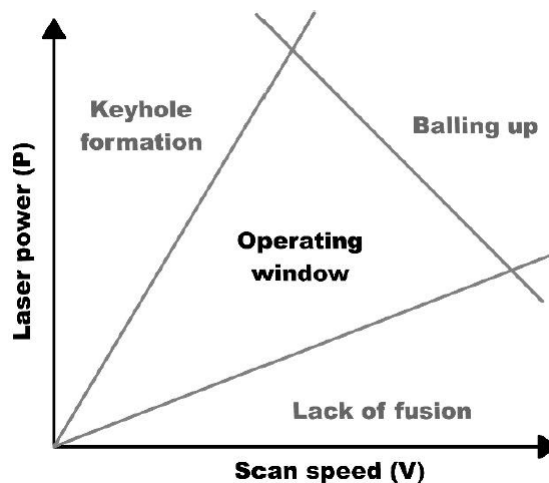
Figure 2.2. Laser power and scan speed operating window [80]

2.1.3   Scan speed

Scan speed of laser beam is another important factor which has a crucial effect on the build time, mechanical properties, surface roughness, and crack generation [37]. Faster scan speeds will reduce the build time. However, at higher SSs, the laser will not have enough time to completely melt/sinter the powder material. To maintain the melt pool consistency at higher SSs, increasing LP or decreasing HS to maintain the same VED will improve the sintering/melting process.
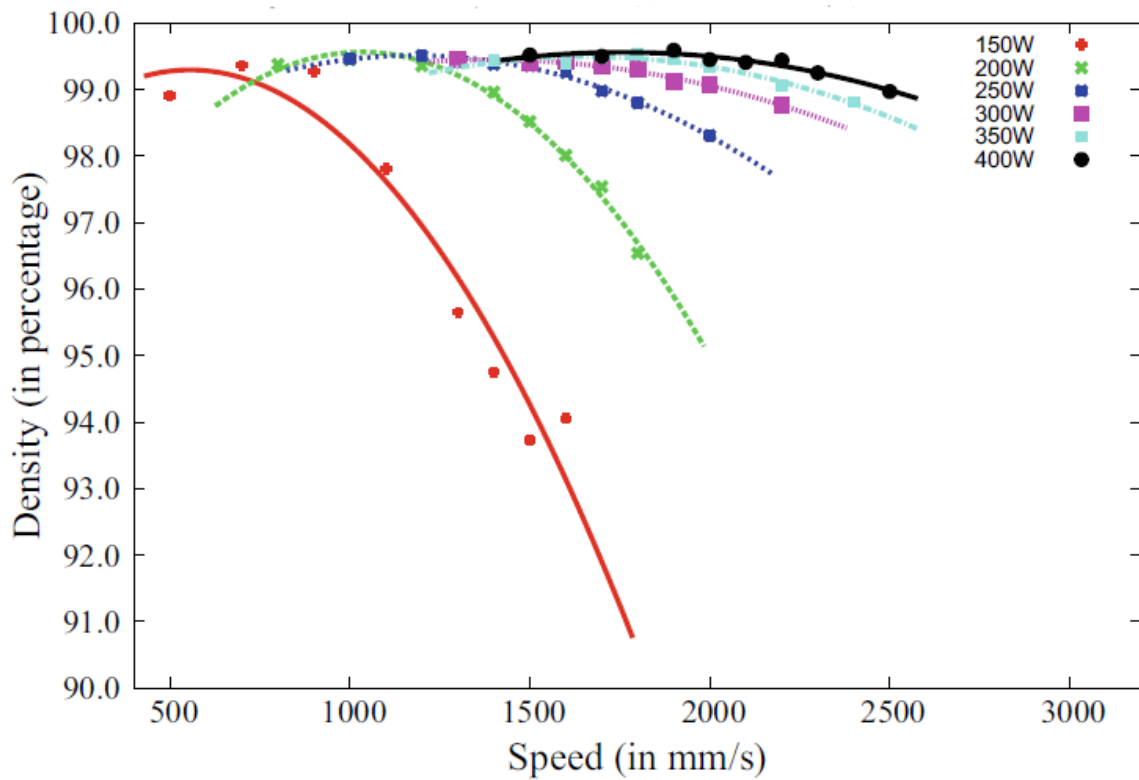
Figure 2.3. Density of 316L SS pillars; LP 150W-400W [38]

The density of the fabricated part is also dependent on the scan speed correlating with VED. At lower laser power working range (<200W), the density of the part drops rapidly with the change in SS fixing the LP constant[38] as shown in Figure 2.3 eventually limiting the range of possible variations of SSs at lower LPs. Due to

melt pool instability at higher SSs, melt splashes occur leading to the formation of micrometer-scaled balling effect on the sintered/melted surface [39] eventually leading to porosity. Also, higher SSs and higher LPs drives to insufficient melting of powder tending to the formation of LOF pores and layers causing crack generation and decreased mechanical properties [37, 40]. Hence, the influence of SS has to be carefully examined for each material along with LP to avoid in-process defect formation.

2.1.4 Layer thickness

Adjusting LT can significantly impact the build rate of the process however, if the layer is too thick, as a result of decreased laser penetration, the melt pool depth decreases and the sufficient bond between two successive layers may not be created leading to the formation of balling. At high LT, microspheres will form on the surface which may retard the deposition of the next successive powder layer or even make the entire process fail. So, uniform powder LT deposition has to be maintained for the entire process. For a thick powder layer, high LP and low SS should be employed for successfully creating the effective melt pool. Significant research has been carried out to study and optimize the effect of LT on the overall process. Typical LT employed in the literature ranges from 0.02mm to 0.1mm. Due to similar microstructure and metallurgical bonding at the LT between 0.02mm-0.04mm, there is no obvious difference/impact of LT on mechanical properties of the fabricated part, but the LT plays an important role on the surface roughness (SR) [41]. At LT >0.05mm, higher plasticity and lower strength properties are observed compared to the LT at 0.03mm *. In this research study, LT was fixed to 0.02mm considering the previous literature works for obtaining the ultimate quality of the fabricated part.

2.1.5 Hatch space

Hatch space (HS) is the distance between two successive laser tracks on the powder layer as the laser passes. Increasing the HS, the overlap between tracks decreases

resulting in insufficient melting/sintering of the powder material leaving some un-melted/unsintered and forming LOF defects. Decreasing the HS increases the over-lap and can result in burning of the edge of laser track. Also, HS significantly effects the VED applied. HS has to be adjusted to an optimal value allowing the required overlap for sufficient bonding as shown in Figure 2.4 between laser tracks and main-taining the VED required according to LP and SS requirements. Depending on the
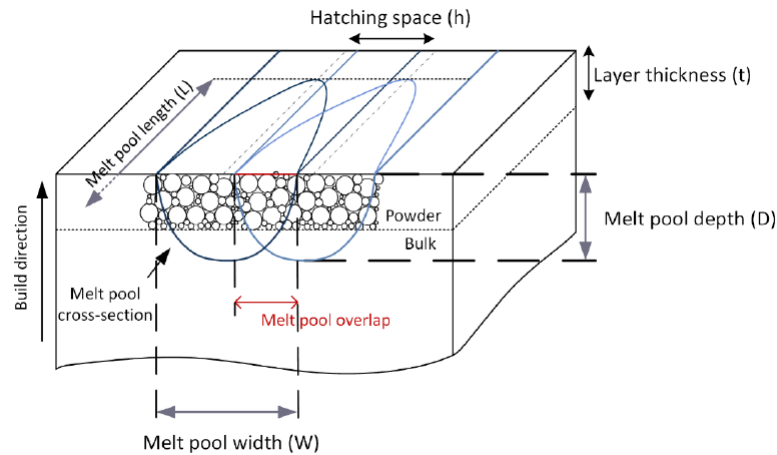
Figure 2.4. Schematic representation of meltpool and process parameters[42]

testing range of LP, SS and HS, the effect of HS on the formation of defects, tensile strength and porosity vary. Scholars demonstrated that HS has the greatest influence in formation of porosity and tensile strength however, few scholars mentioned that HS has no effect on the defect generation and mechanical properties in their working range [41-43]. But the overlap rate significantly affects the melting/sintering process and results in the formation of pores which in turn affects the tensile properties of the fabricated part. A comprehensive study of HS, with wide testing ranges of LP and SS has to be conducted to reach a complete understanding of the importance of HS in PBF process.

2.1.6 Beam diameter

Beam diameter is one of the least studied process parameters due to the limitations of the equipment available in the market. In general, the variable focus diameter ranges from 0.1 mm to 0.5 mm (e.g. EOSINT M 270) for the equipment available in the market. With the limited research available and the equipment license issues
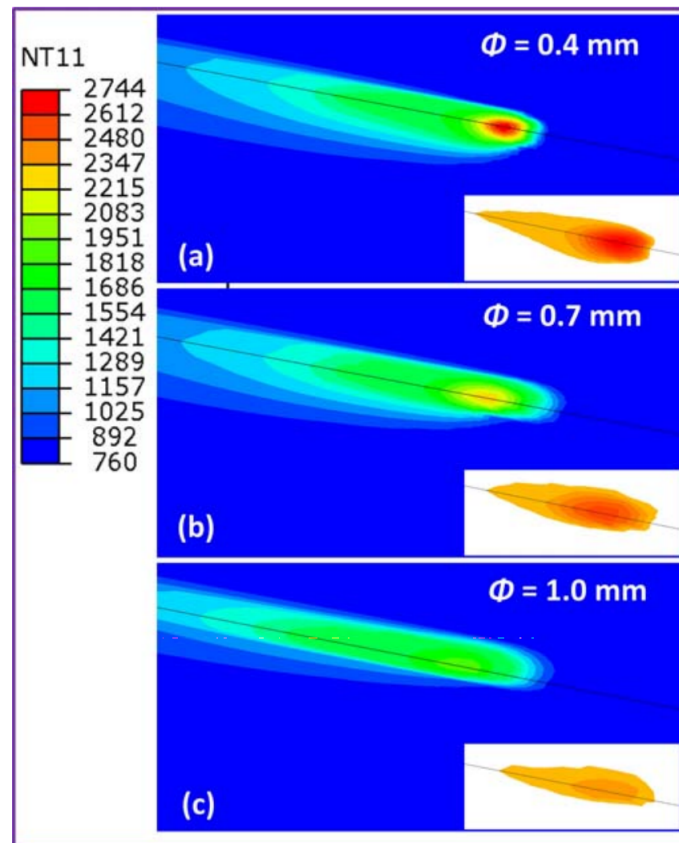
Figure 2.5. Molten pool temperature fields at various beam diameter[44]

manufacturers face, BD was preset to a machines constant value. Taking advantage of the finite element methods (FEM), meager scholars studied the influence of BD on the process. In Shen et al. [44] study, the results show that with an increase in BD, the lower maximum temperature is obtained due to decrease in VED applied at the spot on powder layer as a result, lower cooling rates. However, increasing the BD beyond the optimal value decreases the laser penetration into the powder

layer which can significantly affect the bonding between layers and may lead to LOF defect. Figure 2.5 represents the maximum temperatures reached different BDs. In this research work, BD of 0.1 mm, 0.15 mm, 0.2 mm are tested in the optimal range of VED obtained from the phase-1 of the framework explained in Chapter 3.

2.1.7 Volumetric energy density

Under different combinations of process parameters, VED is often used as a measure for comparing the quality of components manufactured by PBF process. VED is the thermodynamic quantity described as the amount of energy delivered by the laser for a unit volume of powder deposited and is expressed in Eq. (2.1).

$$VED = \frac{P}{S.V.t} \tag{2.1}$$

Depending on the material being used, VED has to be adjusted providing sufficient energy for successfully melting/sintering of the powder into smooth tracks maintaining uniform melt pool dimensions. Lower VED doesnt provide enough energy to completely melt/sinter the powder material consequently forming LOF defects and reduces the density and mechanical properties. Higher VED provides a greater amount of energy which results in evaporation of the powder material and spatters of melted material resulting in the formation of gas pores thereby increasing the porosity and decreasing the quality of the fabricated component. An optimal process window for VED has to be determined for successful melting/sintering of the powder material without any process-induced defects ultimately obtaining a uniform microstructure and better mechanical properties [45]. For any material, VED has to be estimated for achieving the energy required for melting/sintering the powder material and subsequent solidification of the melted material. Chapter 3 demonstrates the methodology used for roughly estimating the VED based on heat per unit volume concept. Extensive research has been conducted by scholars to reach optimal VED range however, same VED can be maintained with a different combination of process parameters

(LP, SS, HS and LT). Limited information can be found on studying the effect different sets of process parameters maintaining the VED value constant. Maintaining the VED constant and varying the process parameters can significantly help in better understanding of the importance/influence of each individual parameter on the melt pool formation, in-process defect generation and ultimate quality of the fabricated part. In this research work, a framework is proposed in which the first phase optimizes the VED and in the second phase, maintain the VED constant, the influence of different ranges of parameters on the quality characteristics of fabricated part is studied for improving the existing knowledge and for creating an optimal system for PBF process. Chapter 3 provides the necessary information and methodology for achieving this objective.

2.2 Process induced defects

In the previous section, the significance of process parameters on the defect generation and ultimate quality of fabricated parts was described. In this section, various process induced defects will be elucidated in detail.

2.2.1 Introduction

In this era of Industry 4.0 and AM, one of the biggest challenges facing metal AM is the formation of process-induced defects which hinders the ultimate properties of the fabricated part from meeting desired manufacturers standard. Changing the process parameters not only influences the microstructural characteristics of the fabricated component, but also results in the formation of process-induced defects which ultimately affects the quality of the AM components. LP, SS, HS and BD are few parameters among all which have a significant influence on the defect formation. Although significant research has been conducted to study the influence of each parameter on the defect formation, the combined influence of process parameters is not optimally studied leading to an incomplete understanding of the correlation between

process parameters and defect formation. From section 2.2.2, process induced defects are categorized and explained with the influence of process parameters in the formation of defects in detail.

2.2.2 Porosity

This is the most regular defect found in AM components. Several process parameters conditions and powder characteristics have an influence on the porosity. The porosity can be seen at different scales i.e. macro, micro and nano range. Macro porosity is the majority scale which can be categorized into gas porosity and LOF.

Gas porosity

Deviations from the optimal VED value results in dynamic changes of melt pool dimensions and enthalpy consequently increasing the potential to trap gas, forming gas porosity. A circular pore is usually identified as the gas porosity. Working with higher VED than required will evaporate the powder material forming gas. Also, the potential for gas entrapment attributes to three main sources namely high powder flow rate, an entrapped gas present in powder material and Marangoni effect. Marangoni flow is the mass transfer due to surface tension along with two fluid interfaces causing gas bubbles within the melt pool. Marangoni flow leads to the formation of gas bubbles in the melt pool which subsequently results in the formation of big pores by the end of the process [46]. Increasing VED will help in reducing/eliminating the micro and nanopores but might lead to other inhomogeneities [47].

Lack of fusion porosity

The inability to sinter/melt the powder material at insufficient/low VED values leads to the formation of LOF porosity in PBF process. Increasing the HS or increasing the BD can cause LOF porosity. In general, LOF defects can be seen along

the layers of boundaries in an irregular shape. Often, LOF pores contain unmelted powder. According to Liu et al., LOF defects can be classified into three groups [48]:

- separated surface with un-melted powder.

- separated surface without un-melted powder.

- narrow and long shaped with unmelted powder.

SS has a major impact on LOF defect formation. Higher SS decreases the specific energy input resulting in incomplete sintering/melting of the powder particles leaving unmelted powder and forming LOF porosity.

2.2.3 Microstructure

Depending on the application, any deviation of features seen in microstructure is considered as a defect. Microstructure anomalies can be seen in the form of variation in crystallographic texture and grain size, LOF, porosity, cracks and composition.

2.2.4 Balling phenomena

Balling is generally seen in the laser sintering process. The primary cause for balling phenomena is the application of low VED which results in insufficient sintering of the powder material. Also, due to the presence of oxygen, oxide layers forms on the solid and molten material changing the wetting process of the material consequently leads to balling [49]. Increasing the LP, decreasing the SS, decreasing the LT ultimately to achieve greater VED can control the formation of balling phenomena during the process. Figure 2.6 shows the schematic of balling phenomena.

2.2.5 Keyhole formation

Keyholes are formed when for a given SS, high LP is used consequently applying greater VED and excess penetration of the laser into the current layer and previous
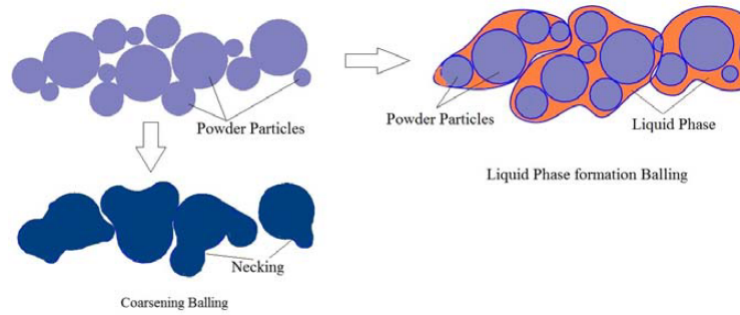
Figure 2.6. Schematic of balling phenomena [37]

layers. Keyholes trap more energy deep inside the cavity leading to the formation of deeper melt pool as shown in Figure 2.7. Also, with the keyhole formation, spatter of powder particles occurs and traps powder inside the cavity.
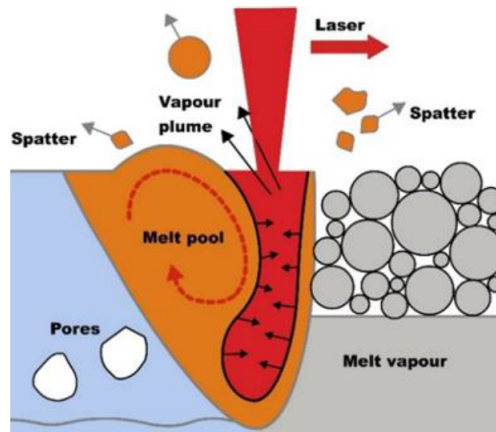
Figure 2.7. Keyhole formation [80]

2.2.6 Crack formation

Different physical phenomena and process parameters can result in the formation of cracks in fabricated AM parts. Merging of melted/sintered powder to the nearest

particles which can either be in solid or liquid phase rather than to the previous layer can cause a thermal energy distribution change leading to the formation of large channels of material resembling cracks in the fabricated part. Also, high thermal gradients in the melt pool during solidification process can lead to the formation of cracks (hot tearing). Figure 2.8 shows the formation of cracks on the scan track [39]. In addition, the unmelted powder can lead to cracking during the fabrication process due to stress concentrations.
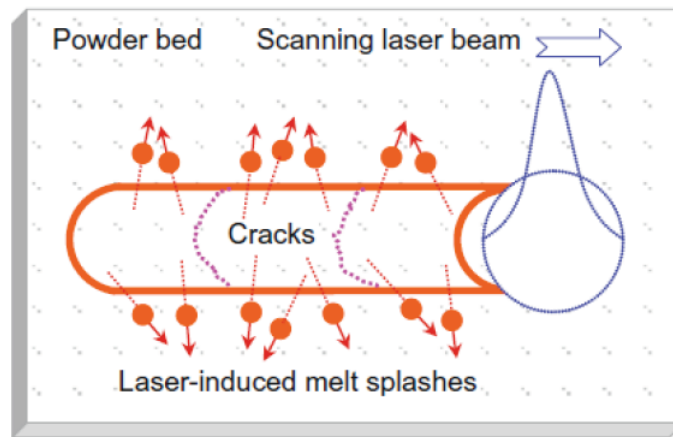
Figure 2.8. Crack formation on scan track [39]

2.2.7 Geometrical anomalies

With applications of AM in various sectors for manufacturing high valued parts, dimensional accuracy is an important quality requirement. Due to the layering process of AM, staircase effect and surface roughness can be formed leading to possible deviations from the actual CAD design. Melt pool dimensions also play a major role in the formation of geometrical anomalies. To minimize anomalies, a stable melt pool shape and size (dimensions) is required [50].

2.3   Research gaps and challenges

With the increasing application of metal AM, quality control has become crucial for obtaining reliance on the adoption into mass production. Although significant research has been conducted to study the PBF process, there are still some gaps and challenges which need to be addressed for achieving better/complete control on the process and for standardizing the process. The current gaps and limitations in the existing literature include

2.3.1   Lacking consistent results

With broader range of research being conducted to understand the effect of process parameters on various phenomena occurring during PBF process and on quality of the part fabricated, inconsistent conclusions/results were obtained by scholars working on the same material and on same equipment. For instance, scholars reported that optimum values of VED for SS316L material was 104 J/mm^3, 70-120 J/mm^3, 70-95 J/mm^3 [33, 35, 45]. Also, for HS, literature demonstrates that it has greatest influence in formation of porosity and tensile strength however; however few scholars mentioned that HS has no effect on the defect generation and mechanical properties [41-43]. These inconsistent results occur because of the different approaches scholars use for obtaining the same end objective. This can be resolved by using a standardized approach/framework.

2.3.2   Multiple parameter consideration

Being a process with more than 50 influential parameters, Changing/controlling all parameters for every build is not realistic/possible. As shown in figure 2.1, the parameters are divided into different categories and controllable parameters have a significant effect on the mechanical properties of the fabricated part. Scholars have been studying the controllable parameters and their influence on the quality charecter-

istics of fabricated part. Limited research attempted to study multiple parameters and their importance on the defect generation and quality charecteristics during the fabrication process and in the best application range of individual process parameters. A comprehensive study considering all the controllable parameters and their influence on the mechanical properties individually and all together has to be conducted for obtaining a better understanding of the process.

2.3.3 Beam diameter

Beam diameter is one of the pre-defined machine specific value which if varied will have significant effect on the heat input at a point [44]. As seen in figure 2.5, BD has a significant influence on the maximum temperatures attained at a spot which impacts the cooling rates and on the laser penetration into the layers for successful bonding between them. Limited knowledge is available on the importance/influence of BD when varied along with controllable parameters and is mostly confined to FE studies without any experimental application.

2.3.4 Lacking a standard approach

The major challenge AM industry is facing is lacking standard procedures and approaches for designing the component, process parameters and for conducting mechanical testing. In the existing literature, to optimize the process parameters, scholars used various approaches leading to inconsistent conclusions/results. In this research, a framework is proposed to address this issue and compare the results with the existing literature.

2.3.5 Lacking a predictive model

In this era of industry 4.0, smart manufacturing plays a crucial role and to achieve this using AM, the process parameters have to pre-designed accordingly with the de-

sired output properties. For achieving this objective, a predictive model has to be developed which is not present in the existing literature for coming up with parameter combination according to the manufacturers/users end-application requirement. With a predictive model, based on the specific needs of the part under fabrication, process parameters can be designed beforehand.

3. METHODOLOGY: IMPLEMENTATION OF THE PROPOSED FRAMEWORK FOR CORRELATING PROCESS-MATERIAL-PROPERTY

The literature review in chapter 2 shows that in-process defects such as porosity, crack formation etc. are the most prevalent defects, with which manufacturer encounter. Also, the previous chapter explains in process induced defects section that laser power, scan speed, hatch spacing and VED are the main contributing parameters for the formation of defects during the fabrication process. The formation of defects leads to decrease in density with irregular porosity distribution which in turn affects the mechanical properties and quality characteristics of the fabricated part. In this chapter, we implement the proposed framework (refer to Figure 3.1) by dividing into two phases. First, we conduct some preliminary experiments to achieve more insight into densification and the effect of parameters on porosity formation with the objective of achieving a maximum density with minimum porosity. These experiments provide the optimized values of VED to implement in the next phase and study the effect of a set of process parameters on the mechanical and quality characteristics of the fabricated part. The objective of this phase is to understand the correlation between process, material and property and ultimately to achieve a part with required quality characteristics. The results from this chapter will be employed in chapter 4 for developing a neural network for training a predictive function of process parameters for the required quality properties of the end-product.

3.1   Proposed framework

To address the aforementioned challenges and gaps, a two-phase framework is proposed for establishing the correlation between process parameters and ultimate
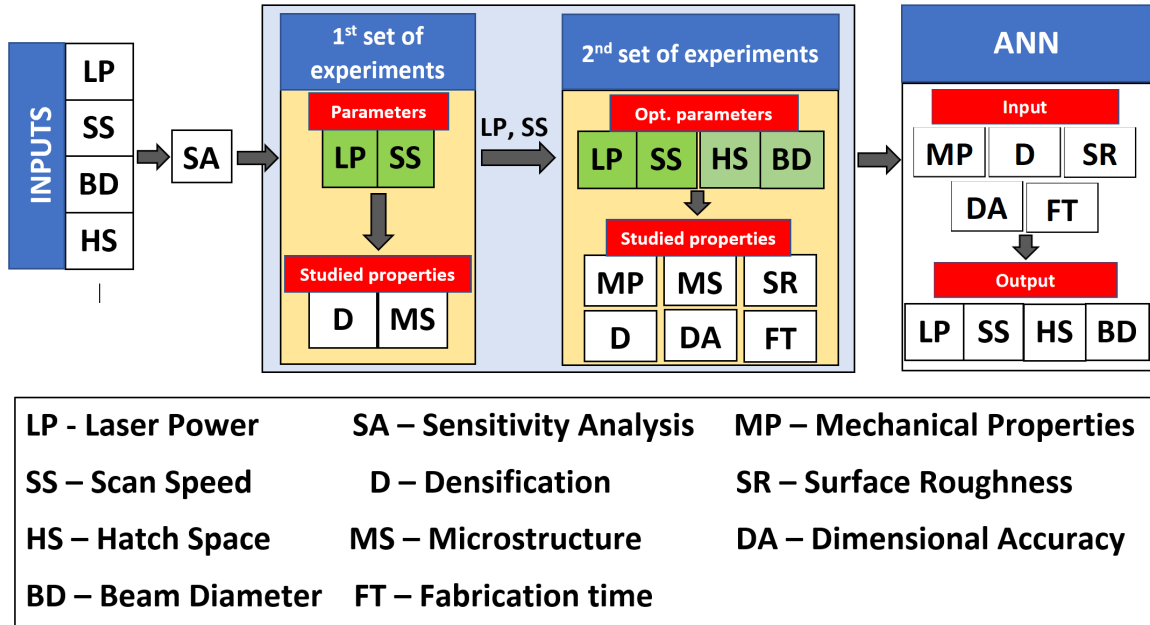
Figure 3.1. Proposed framework and corresponding workflow for developing ANN model

properties of the fabricated part. Figure 3.1 shows the proposed framework. This objective of this framework is to standardize the approach of studying the process parameters which reduces the inconsistency in results for a given material and to develop a predictive function for intelligent selection of process parameters according to the desired quality properties for the part fabricated.

3.2 Phase-I

3.2.1 Introduction

In this section, the first phase of the framework (refer Figure 3.2.) will be explained sequentially and the methodology for implementing will be detailed with emphasis on the obtaining optimum range which will be carried forward in the framework and will be employed in the second phase as input for designing the experiments. With

merely considering laser power and scan speed, the main objective of this phase is to acquire the maximum density parts thereby obtaining the VED range at which maximum densification can be achieved. This VED range obtained will be employed in the next phase for studying the effect of process parameters on the mechanical and quality characteristics of the fabricated part within the maximum densification range.
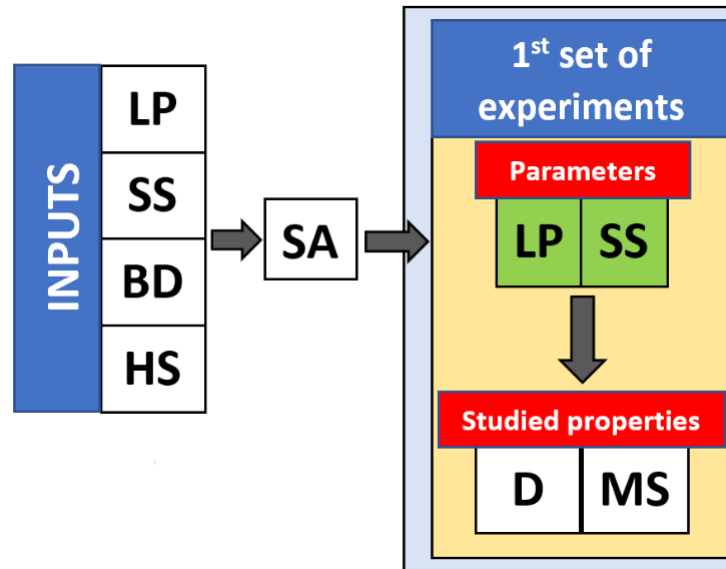
Figure 3.2. Phase I of proposed framework

3.2.2 Material

316L stainless steel is the for this research. The alloy composition and actual specifications as supplied are shown in Table 3.1. 316L SS has widespread application in additive manufacturing due to its good tensile strength at high temperatures, low stress to rupture, high hardness, toughness and corrosion resistance properties [31].

Table 3.1. Composition of 316L SS [33]

Grade 316L	Min	Max	Actual
Carbon, C	-	0.03%	0.019%
Silicon, Si	-	0.75%	0.67%
Manganese,Mn	0.03%	<0.1%	<0.08%
Phosphorus, P	-	<0.025%	<0.019%
Sulphur, S	-	<0.01%	<0.006%
Chromium, Cr	17.5%	<18%	<17.9%
Nickel, Ni	12.5%	<13%	<12.7%
Molybdenum, Mo	2.25%	<2.5%	<2.36%
Nitrogen, N	-	<0.1%	<0.06%
Copper, Cu	-	<0.5%	<0.2%
Oxygen, O	-	<0.1%	<0.022%
Iron, Fe	Balance	Balance	Balance

3.2.3 Mathematical modelling

For any AM process, the starting step is determining the approximate process parameters for successful completion of the fabrication process. This can be achieved by evaluating the VED i.e. amount of heat given per unit volume which is required for sintering/melting of the powder feedstock. Substantial research has been conducted by scholars to comprehend the best range or values of VED for stainless steel 316L. Diversified range of values were obtained by scholars lacking the uniformity in the results for the same material processed with PBF process. In order to understand and address the issue of non-uniform results for VED, in phase I, a rough estimation of VED was calculated and experiments were carried out to obtain the optimized VED range for achieving maximum density. A rough VED that is required for melting and consequent solidification can be estimated based on the heat per unit volume, q

$(\frac{[}{J}]mm^3)$ for successful heating and melting of the material is given by Equation 3.2 [51].

$$\Delta T = T_m - T_0 \tag{3.1}$$

where T_m (K) and T_0 (K) are the melting temperature of the material and room temperature.

$$q = [c.\Delta T + l_f]\rho \tag{3.2}$$

where c $(\frac{J}{Kg.K})$ is the specific heat capacity, l_f $(\frac{J}{Kg})$ is the latent heat of fusion and ρ $(\frac{Kg}{mm^3})$ is the density of the powder material respectively.

However, in order to consider various thermal phenomena [52] associated with PBF process, an efficiency coefficient n is incorporated which include heat losses due to the reflectivity of the powder, heat conduction and additional losses. Equation 3.3 shows the VED equation with the efficiency coefficient.

$$VED = \frac{q}{\eta} = \frac{q}{(1 - R_{Powder})(1 - k_{rel})\eta^*} \tag{3.3}$$

where R_{Powder} and k_{rel} are the reflectivity of the feedstock material expressed in fractions and relative thermal conductivity of the feedstock material. η^* is the additional efficiency factor and is assumed as 0.20 [51].

Table 3.2. Property values for SS316L

Property	Value
specific heat capacity, c $(\frac{J}{Kg.K})$	500
melting temperature, T_m (K)	1673
latent heat of fusion, l_f $(\frac{J}{Kg})$	0.25
Density, ρ $(\frac{Kg}{mm^3})$	7.99 x 10^{-6}

$$q = [500(1673\text{-}296) + 0.25](7.99 * 10^{-6}) = 5.5 \; \tfrac{J}{mm^3}$$

$$\text{VED with } R_{Powder}, \ 0.05 = \frac{5.5}{(1-0.05)(1-0.5)(0.20)} = 57.89 \ \frac{J}{mm^3}$$

$$\text{VED with } R_{Powder}, \ 0.6 = \frac{5.5}{(1-0.6)(1-0.5)(0.20)} = 137.5 \ \frac{J}{mm^3}$$

The VED values obtained here are taken as the lowest and highest limit for the design of experiments (DOE) explained in next sections in which the VED will vary $\pm 10\%$ in order to consider the approximations of the properties introduced.

3.2.4 Sensitivity analysis

Sensitivity analysis (SA) quantifies the correlation between the given model and its input parameters [53]. The main objective of conducting SA is to understand (1) which parameters require additional research for strengthening the knowledge base, thereby reducing output uncertainty; (2) which parameters are irrelevant and can be eliminated from the final model;(3) which inputs contribute most to output variability; and (4)which parameters are most highly correlated with the output [53].
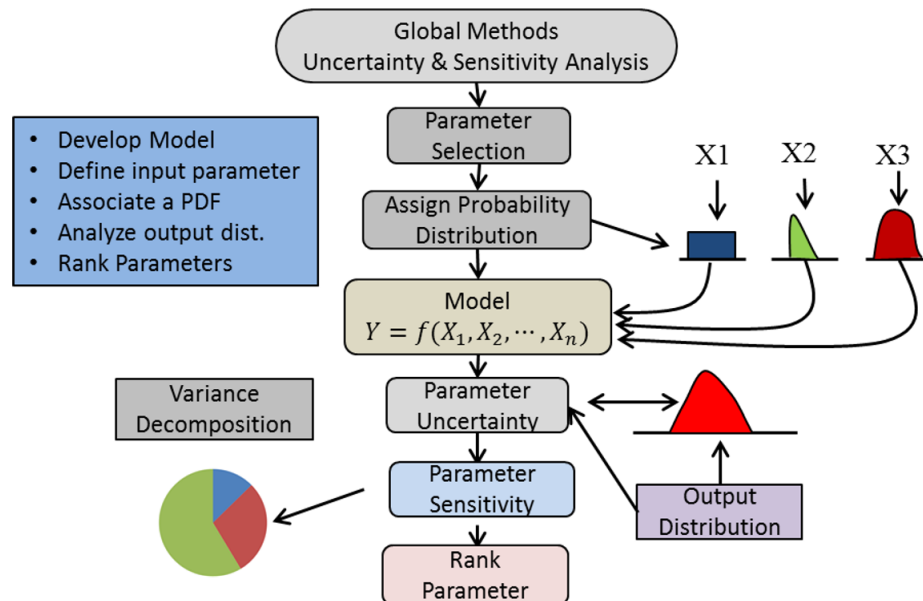
Figure 3.3. Schematic for global sensitive analysis [34]

LP, SS, LT, HS and BD are commonly cited in the literature as the crucial controllable parameters in the PBF process influencing the ultimate quality of the fabricated part [24-27, 54-57]. SA considers these five parameters to evaluate their correlation with the volume-based energy density (ED) shown in equation 2.1 [58]. In this research, LT is set to a constant value of 0.02 mm. However, the employment of SA is crucial to demonstrate the sensitivity of each parameter within the working range in this work. The sensitivity analysis guides us through selecting the levels of parameters and their distribution for designing the experiments during the next step. Figure 3.3 shows the schematic process of global SA employed by MATLAB [59]. Fourier amplitude sensitivity testing (FAST) variable based global method which is based on conditional variables for determining the uncertainty. The SA results evidently show the scan speed as the most sensitive parameter, which drastically changes the energy
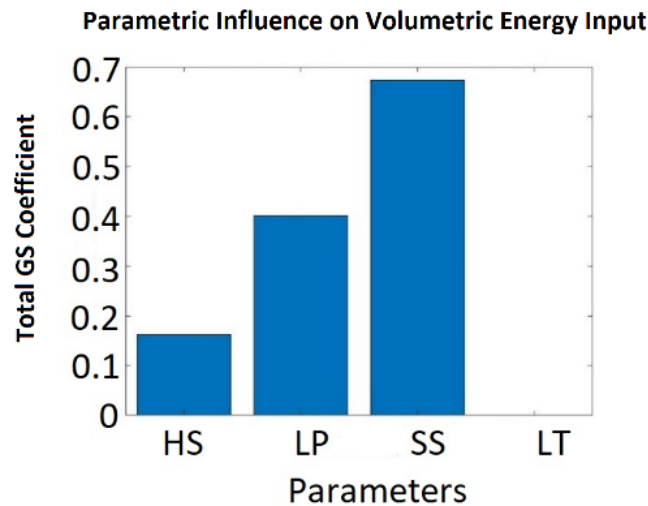
Figure 3.4. Total Global Sensitivity (GS) Coefficient

applied per volume and might influence the ultimate properties of the fabricated part predominantly [58]. In a similar way, the laser power and hatch spacing also have a considerable effect. The effect of layer thickness is not calculated as it is set to a constant value throughout this research. figure 3.4 shows the values of the total

global sensitivity coefficient obtained by SA. Previous literature also confirmed the significant influence of laser power and scan speed, as two main parameters that affect the energy transferred to the powder, on the ultimate quality of the printed part [8].

3.2.5 Design of experiments

In this phase, for designing experiments, full factorial analysis is employed and the experiments were manufactured on LPBF machine EOS M280 with maximum laser power of 200W. Table 3.3 shows the parameters, namely, LP and SS, whose values are assigned based on the VED estimations calculated in section 3.1.3 and literature [16, 55, 58] and Table 3.4 shows the full factorial DOE. The first set of experiments prints a 10mm10mm5mm samples (figure 3.5) considering merely the LP and SS, while HS and BD are kept constant at their machine default values (HS = 0.09 mm and BD = 0.09mm). The LT is also set to a constant value of 0.02 mm throughout the work. In this phase, we study the microstructure, porosity, and densification of the printed samples to map them onto the VED. Previous literature demonstrated that the porosity generated in the during the process significantly affects the mechanical properties of a fabricated part. The porosity formation in low ranges (near full density parts) is seen to alter mechanical properties substantially [60]. Moreover, reducing the porosity enhances the build consistency [61]. Thus, in this phase, we seek to obtain the optimal range of energy density for maximum densification. It should be noticed that we study only 13 samples due to very close energy density for four of the samples.

Table 3.3. Control factors and levels for DOE

Factor	Level values	Levels
Laser Power, W	100, 125, 150, 175	4
Scan Speed, mm/sec	700, 800, 900, 1000	4

Table 3.4. Full factorial DOE

No.	Laser power (W)	Scan speed (mm/s)	No.	Laser power (W)	Scan speed (mm/s)
1	100	700	9	150	700
2	100	800	10	150	800
3	100	900	11	150	900
4	100	1000	12	150	1000
5	125	700	13	175	700
6	125	800	14	175	800
7	125	900	15	175	900
8	125	1000	16	175	1000
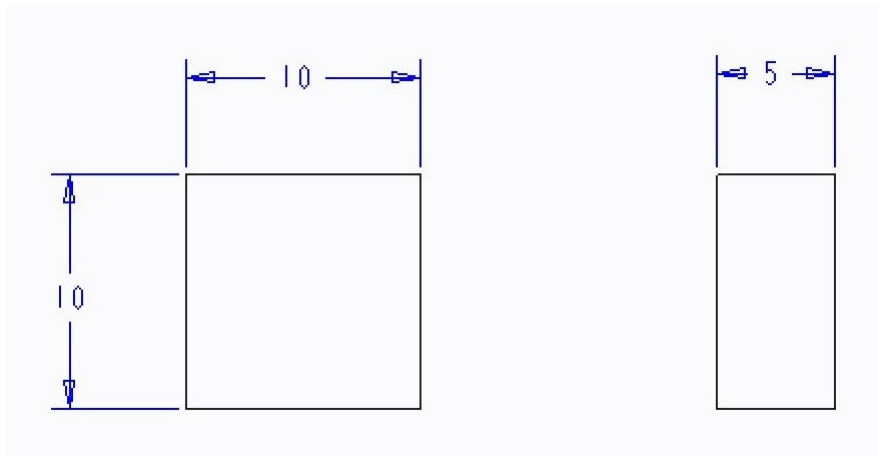
Figure 3.5. Dimensions of sample in phase-I

3.3   Phase-II

3.3.1   Introduction

From the phase-I (section 3.2), the optimized VED range for achieving maximum densification is obtained. In the second phase, LP, SS, HS and BD will be studied to understand the correlation between process parameters and the mechanical and quality properties of the fabricated part (figure 3.6). In the following subsections, a detailed explanation of the parameter selection, DOE, mechanical testing, analysis

of the data will be presented. A comprehensive elucidation of the mechanical testing with the details of equipment used and the equipment settings will be presented along with the steps for completion of the framework.
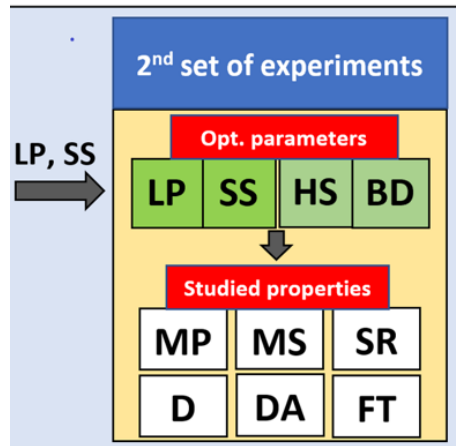
Figure 3.6. Phase II of proposed framework

3.3.2 Design of experiments

As four process parameters are being considered with different levels in this phase, conducting a full-factorial analysis requires fabrication of many samples, material and a great deal of time. Instead of conducting a full-factorial analysis, Taguchi method is used to design experiments. Taguchi method is a statistical method, which designs experiments using Orthogonal Array (OA) technique to eventually improves the quality of a manufacturing process [26]. The OA technique converts the parameter design values to the S/N ratio and calculates the design robustness [18]. To improve the product quality, the quality characteristics must deviate as little as possible from the target value. OA is a systematic and statistical way of testing interactions between control factors. It provides a uniformly distributed set of experiments, which covers all the paired combinations of the variables instead of the full factorial analysis. Table 3.5 shows the assigned levels and values for the process parameters based on

the results obtained from phase-I and table 3.6 shows the Taguchi DOE. Samples for tensile, impact and hardness test are fabricated for each set of parameters in DOE. Tensile and impact samples are designed according to the ASTM E8 and ASTM E23 standards [65](Table 3.8). Figure 3.7 shows the dimensions of fabricated samples.

Table 3.5. Control factors and levels for taguchi DOE

Factor	Level values	Levels
Laser Power, W	125, 150, 175, 195	4
Scan Speed, mm/sec	700, 800, 900, 1000, 1100, 1200	6
Hatch space, mm	0.09, 0.12, 0.15	3
Beam diameter, mm	0.1, 0.15, 0.2	3

Table 3.6. Taguchi DOE

No.	LP (W)	SS (mm/sec)	HS (mm)	BD (mm)
1	125	700	0.09	0.1
2	125	800	0.09	0.2
3	150	700	0.12	0.15
4	150	800	0.09	0.2
5	150	900	0.09	0.1
6	175	700	0.12	0.2
7	175	800	0.12	0.1
8	175	900	0.09	0.15
9	175	1000	0.09	0.2
10	175	1100	0.09	0.1
11	195	700	0.15	0.15
12	195	800	0.12	0.15
13	195	900	0.12	0.2
14	195	1000	0.09	0.1
15	195	1100	0.09	0.2
16	195	1200	0.09	0.15

Table 3.7. Tensile testing specimen, ASTM E8/E8M 13a [31]

Dimensions for the subsize specimen (6 mm [0.250 in.] wide) (mm [in.])	
G Gauge length	25.0 0.1 [1.000 0.003]
W Width	6.0 0.1 [0.250 0.005]
T Thickness	Maximum 6 mm
R Radius of fillet, min	6 [0.250]
L Overall length, min	100 [4]
A Length of reduced section, min	32 [1.25]
B Length of grip section, min	30 [1.25]
C- Width of grip section, approximate	10 [0.375]

3.3.3 Signal-to-noise ratio and analysis of variance

The signal/noise (S/N) is a method of variability measurement of the manufacturing process, which evaluates the process parameters at all individual levels and ensures the resulting optimum process conditions are robust and stable. The following equations calculate three types of S/N ratios, namely, the lower-the-better used for surface roughness (Equation 3.4), the higher-the-better used for mechanical properties (Equation 3.5), and the nominal the better used for dimension accuracy (Equation 3.6) [18, 54].

$$\frac{S}{N} = -10 * log_{10}\left(\frac{1}{n}\sum_{i=1}^{n} Y_i^2\right) \tag{3.4}$$

$$\frac{S}{N} = -10 * log_{10}\left(\frac{1}{n}\sum_{i=1}^{n} \frac{1}{Y_i^2}\right) \tag{3.5}$$

$$\frac{S}{N} = -10 * log_{10}(s^2) \tag{3.6}$$

where n is the number of measurements and Y_i is the observed performance characteristic value and s is the standard deviation of the responses for the given factor level
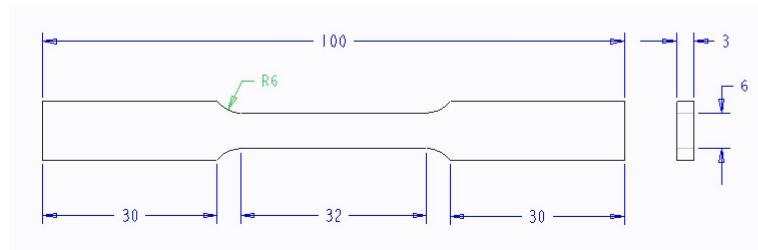
(a) Tensile
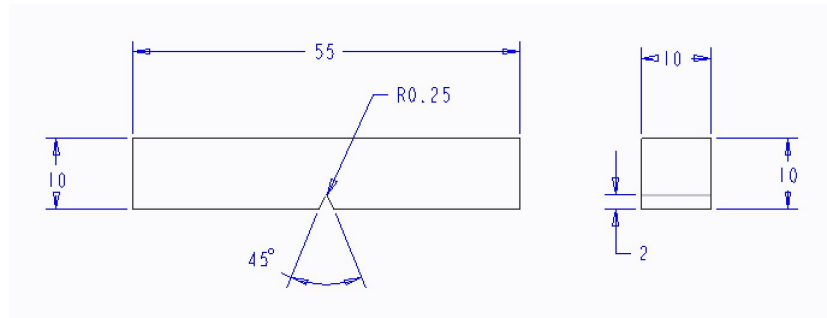
(b) Impact
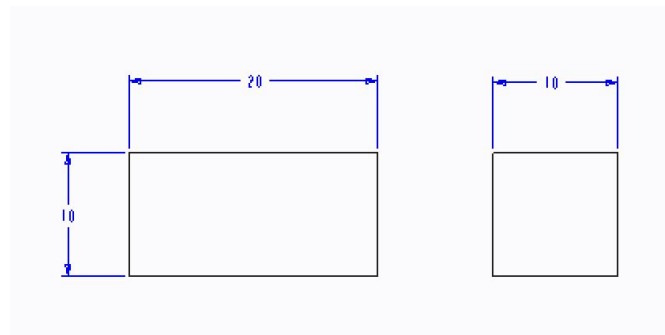
(c) Hardness

Figure 3.7. Designed specimens

combination. S/N value will be calculated in this phase for all 16 experiments. With the factor of having 16 experiments, even the slightest variation/error in employing S/N value can be identified when the resulting S/N values will be used for calculating the variance. After the calculation of S/N value, a method called Analysis of Variance (ANOVA) statistically evaluates the significance of the control factors (i.e. process parameters in this work) and their influence on the experimental results (mechanical

properties). ANOVA studies the variance of properties with the levels of parameters by employing the data available after material and mechanical testing [66]. The provided graphs and distribution charts will describe the variance of properties within the tested range of levels; thus, they will obtain the optimal range of the values for SS 316L in the PBF process. S/N ratio is calculated for each parameter at their individual levels and is graphically represented for each parameter. This graphical representation gives an insight into the effect of each parameter on the quality characteristics of the fabricated part. After calculation of the S/N value, ANOVA method is used to analyze the significance of individual parameters on the end-quality properties with a series of calculations which will be demonstrated in section 4.2 and finally comes up with the percentage contribution of the process parameters for each property. This will complete the correlation between the material, process and properties for the PBF process, which will guide in the development of an ANN system.

3.3.4   Mechanical testing

To complete phase-II to understand the correlation between process parameters and quality properties of the part fabricated, a series of mechanical testings are conducted. As shown in figure 3.6, microstructure, surface roughness, porosity, dimensional accuracy, tensile, impact and hardness tests have to be conducted. Due to limitations of equipment, at this moment, only surface roughness, hardness and impact tests are conducted and the results will be explained in chapter 4.

Surface roughness

The surface roughness R_a measurement is carried out on Bruker DektakXT system shown in figure 3.8. A stylus of 2μm radius is used with the profile set to hills and valleys and with a range of 6.5μ, the force of 5mg, speed of 600 μ m/s and time duration of 25 seconds. On each sample three readings were taken from two corners and center with the scan length of 10mm.
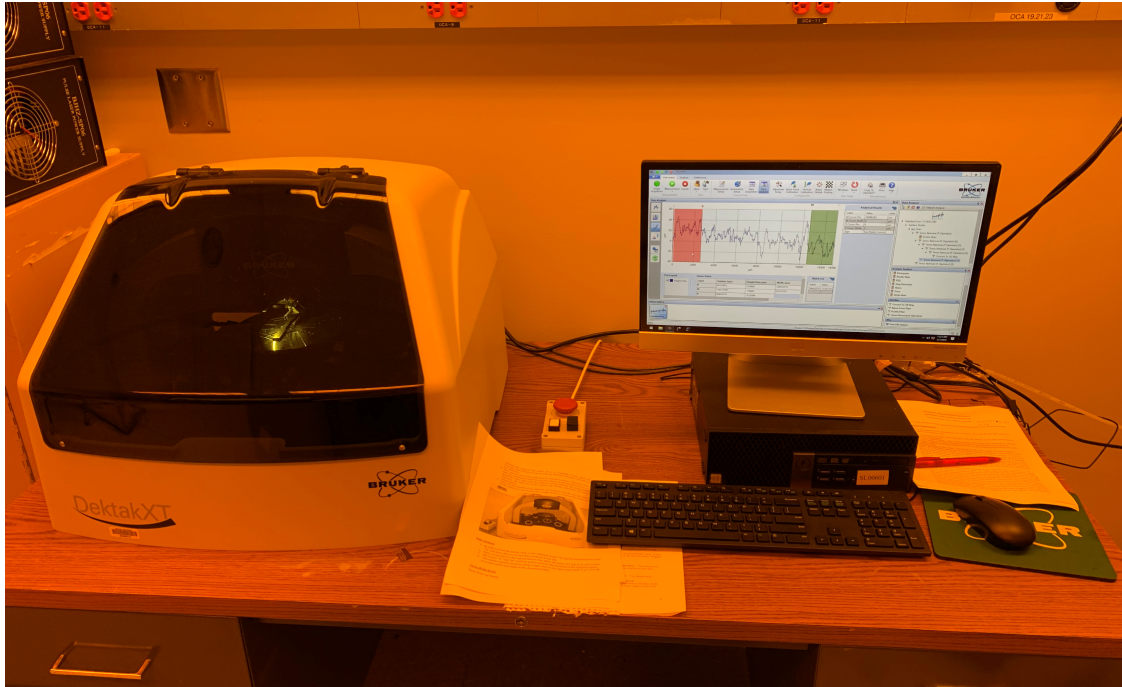
Figure 3.8. Bruker DektakXT

$$R_a = \frac{1}{L} \int_0^L |Y(x)| dx \qquad (3.7)$$

where R_a is the surface roughness which is the arithmetic average deviation of hills and valleys from the mean line, L is the scan length and Y(x) is the profile of the curve.

Hardness

The hardness test typically is a non-destructive test with minimal destruction of the sample. It is conducted on Rockwell hardness testing machine B scale which is equipped with 1/16 inch steel ball. A force of 100Kgf is applied. Figure 3.9 shows the Rockwell machine. By conducting hardness testing, more insight into resistance of material for plastic or permanent deformation can be obtained. With samples fabricated with different sets of parameters, conducting hardness test can help to study the effect of process parameters on the ductility and brittleness properties.

Figure 3.9.   Rockwell testing equipment

Charpy impact test

Samples are fabricated using ASTM E23 standard dimensions as shown in figure 3.7. Figure 3.10 shows the charpy impact test equipment. The specimen is loaded and the position of the specimen is adjusted such that the notch is parallel and centered to the pendulum. The pendulum is dropped electronically to avoid any losses due to vibrations which might occur if dropped manually. The equipment is not bolted to the ground which might effect the results obtained by $\pm$ 5. The objective of conducting the impact test is to study the amount of energy absorbed and to study the effect of process parameters on the fracture growth or break of the sample giving insight into plastic deformation.

Figure 3.10.   Impact testing equipment

4. RESULTS AND DISCUSSION

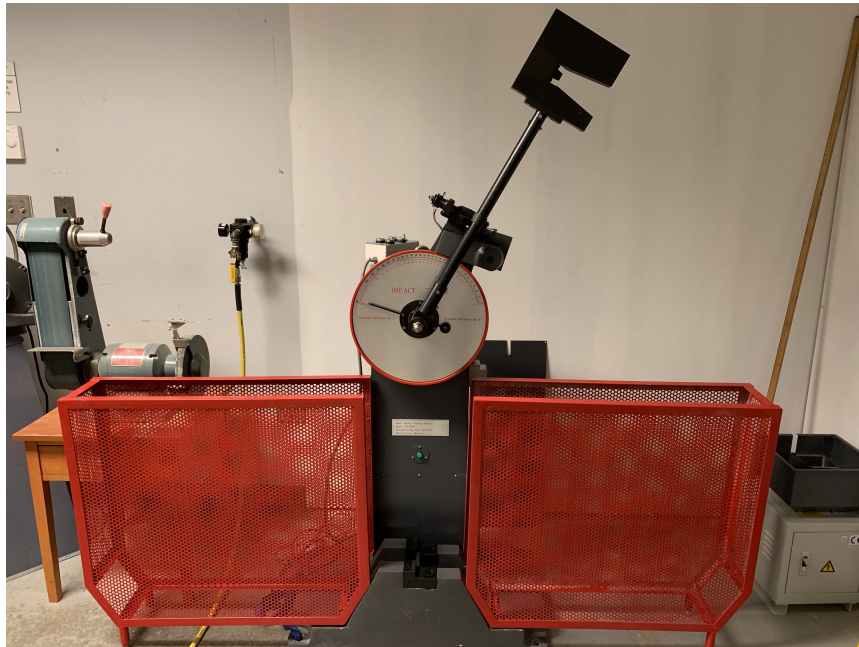In chapter 3, the methodology for implementing the two phases in the framework is explained. In this chapter, the results obtained after implementing each phase is elucidated with detailed discussion on the results obtained for establishing the correlation between process parameters and quality properties of the part fabricated. Finally, the data to be used for developing a predictive function (chapter 5) will be explicated.

4.1 Phase-1: Results and discussion

From the mathematical model explained in section 3.2.3, the minimum and maximum values obtained for VED are 57.89 J/mm^3 and 137.5 J/mm^3. SA is conducted to study the influence of LP, SS and HS on VED applied and the results evidently showed that SS has the major influence on the VED applied followed by LP and HS in the working range of VED (refer figure 3.4). After SA, DOE is conducted and 16 samples were printed with 10 x 10 x 5 mm dimensions (refer figure 3.5). We cut each of the samples in the first set of experiments from the center in both directions, namely, perpendicular to the build direction and parallel to the build direction (Figure 4.1) by using wire electric discharge machining (WEDM) process. WEDM process is chosen because of its capability of machining hard materials which are electrically conductive without inducing any stresses or impact which is an added advantage.

We take sixteen micrographs in total from each sample by using a scanning electron microscope (SEM). Six micrographs are taken from the horizontal cross-section (each corner plus two from the center area) and two from the vertical one (Figure 4.2), each uses two different magnifications i.e. 60X and 300X (100μm and 10μm scale respectively). We employ the MATLAB image processing to measure the porosity
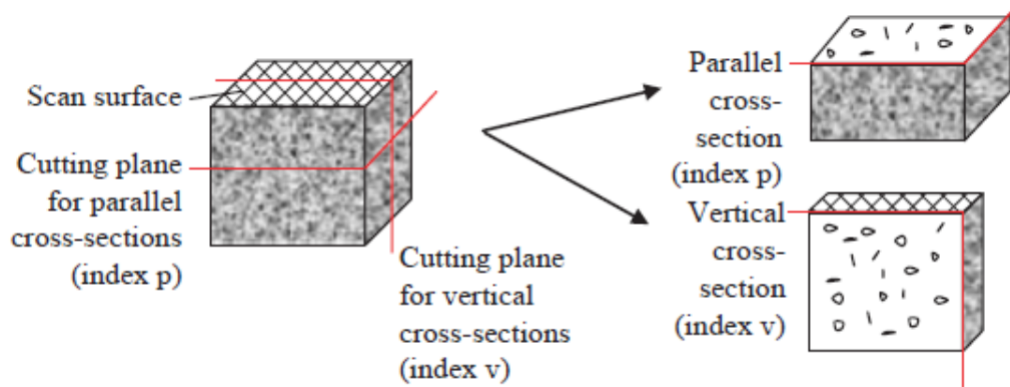
Figure 4.1. Cutting planes in the specimens of the phase-I [40]

(a) Horizontal   (b) Vertical
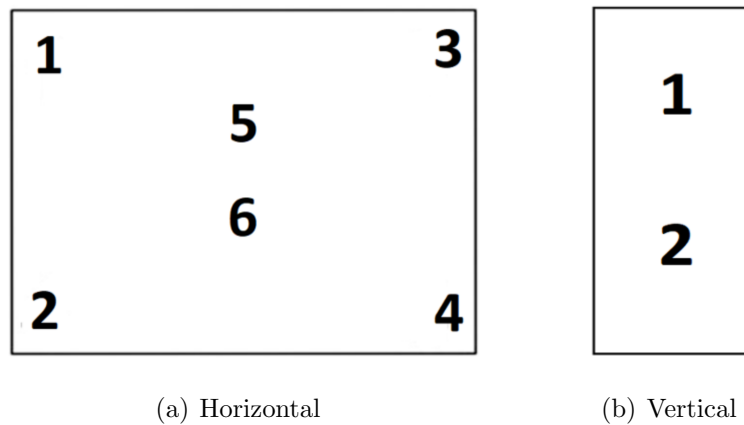
Figure 4.2. The positions of image captured on cross-sections

of each sample in two steps. First, MATLAB creates black and white (BW) images from the micrographs. In these images, the black pixels represent the porosity and the white pixels represent the solid. In this step, the threshold level is adjusted by comparing the pore size in the SEM image (Figure 4.3 (a)) with the image generated by MATLAB (Figure 4.3 (b)) to increase the accuracy of the method [62]. Then, we calculate the ratio of the number of black pixels to the total pixels for the horizontal BW micrographs and the vertical ones separately. The overall average ratio for both magnifications on the BW images of horizontal cross-section and vertical cross-sections represent the porosity value of the printed sample in each direction.

(a) SEM image   (b) MATLAB image
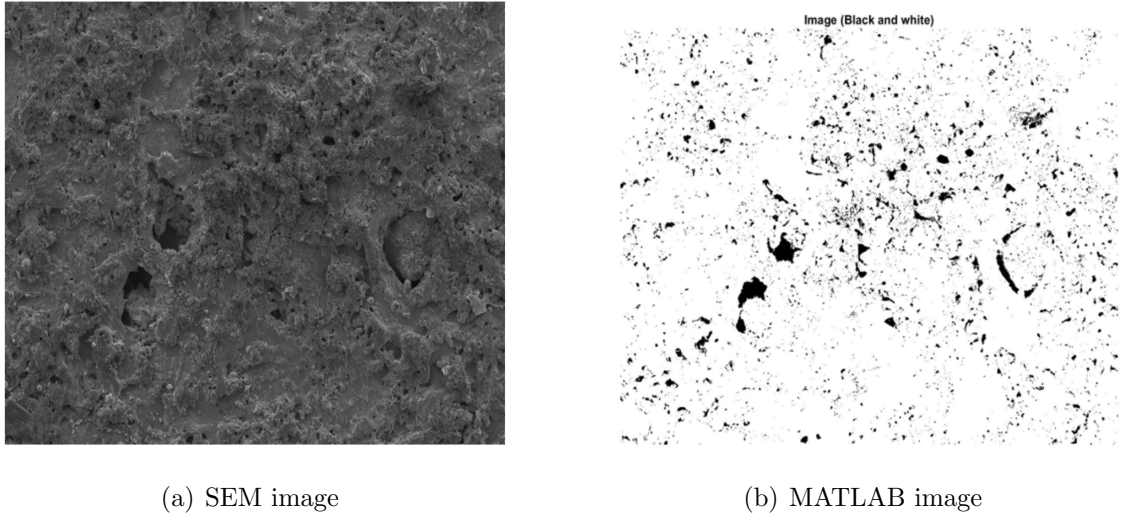
Figure 4.3. The positions of image captured on cross-sections

The horizontal cross-section micrographs of the samples from the first set of experiments show the energy densities applied to the samples generate three different types of porosity according to low, medium, or high value of VED. Low VED leads to incomplete melting of the powder particles and formation of irregular pores due to lack of fusion such as sample 3 (the low VED with LP 100 W and SS 900 mm/s) (Figure 4.4 (a)). While, the exertion of high volumetric energy vaporizes the material and hence, it leads to the formation of circular gas pores such as sample 13 (the highest VED with LP 175 W and SS 700 mm/s) (Figure 4.4 (b)). These circles can be a cross-section for a keyhole porosity. Samples with medium VED such as sample 16 (medium VED with LP 175 W and SS 1000 mm/s) possess microscale holes with a nearly uniform distribution throughout the cross-section, which is an evidence in better mechanical properties compared with the other types [63]. Table 4 illustrates the porosity values of the three aforementioned samples. The results are confidently in agreement with the results from the previous literature such as cherry et. Al. [64]. Different types of porosity are visible in horizontal and vertical cross sections, which lead to different porosity percentage in each cross section. Vertical cross-sections illustrate the less frequent but bigger size porosity usually progressing through layers.
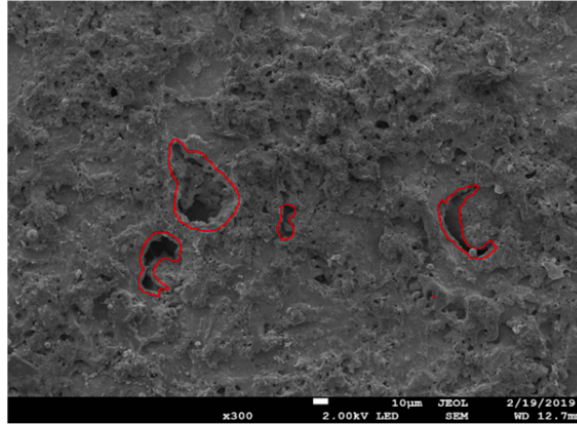
(a) LOF pores
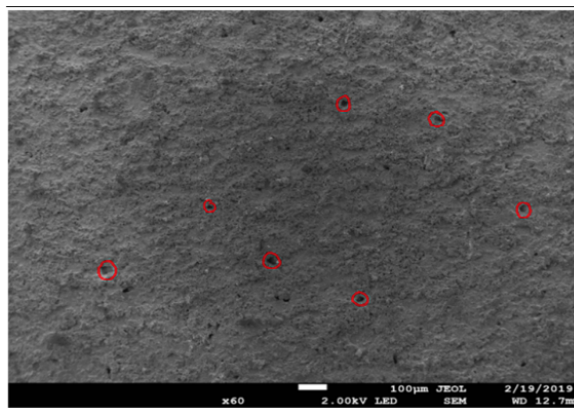
(b) Gas pores

Figure 4.4. Different pores formed during the process

Table 4.1. Porosity of the samples

Sample	Horizontal (%)	Vertical (%)	Porosity (%)
3, VED = 61.7 J/mm^3	5.453	3.5	4.48
16, VED = 97.2 J/mm^3	0.8793	0.502	0.69
13, VED = 138 J/mm^3	1.8736	1.308	1.59

Whereas, horizontal cross-sections illustrate the widespread porosity in different size ranges, which scatters throughout the entire section (Figure 4.5). The horizontal porosity will be used in the future phase of this framework.
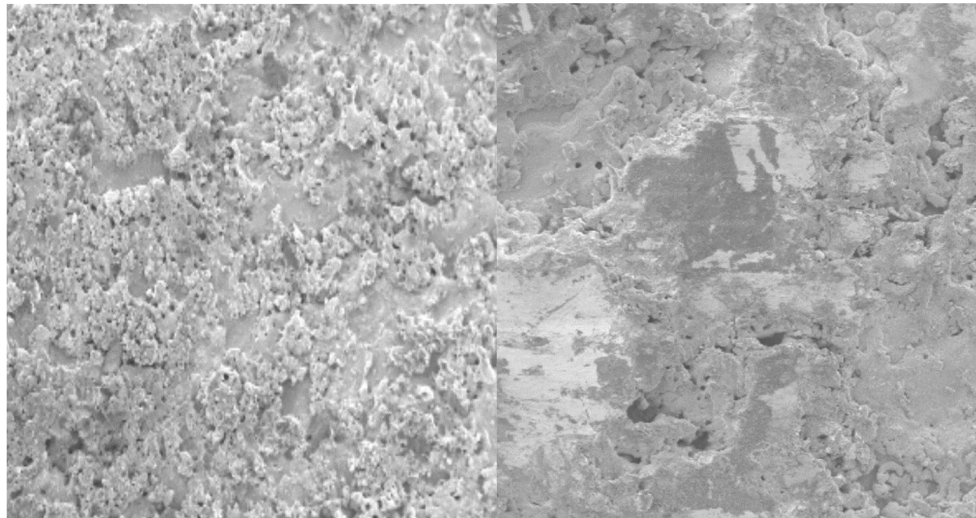
Figure 4.5. Horizontal vs vertical cross-section SEM images
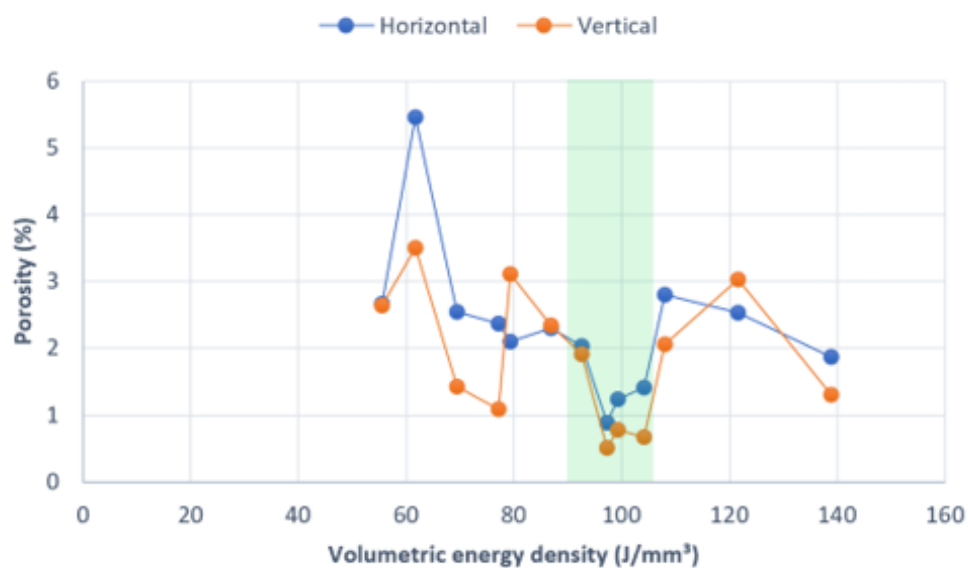
Figure 4.6. Porosity vs VED

The porosities in horizontal and vertical cross-sections for the samples according to the applied VED is shown in figure 4.5. As figure 4.6 shows, the energy density alters between 55 and 138J/mm3. This energy density creates a part with the density between 95.52% and 99.31% with a maximum of 99.31%. The maximum density is

achieved with the VED of 99.2 and 104.17J/mm3. Considering the densification percentage, we can narrow down the range of optimum VED to 90 J/mm^3 and 105 J/mm3 shown in the green band in figure 4.6. This range of VED suggests the optimized range between 150 W to 200 W for the laser power and 800 mm/s to 1000 mm/s for scan speed to obtain the maximum densification. These ranges will be employed as the inputs for the second phase in the framework. The second phase will study the correlation between material, process parameters (LP, SS, HS and BD) and ultimate quality characteristics of the fabricated part in the maximum densification range.

4.2   Phase-II: Results and discussion

4.2.1   Surface roughness

As explained in section 3.3.4, surface roughness measurement is conducted on Bruker DektakXT system and three readings of 10 mm scan length are recorded and averaged to obatin the R_a value for each sample. From the profile shown in figure 4.7, mean value of hills and peaks and R_a value is calculated from the equation 3.7.
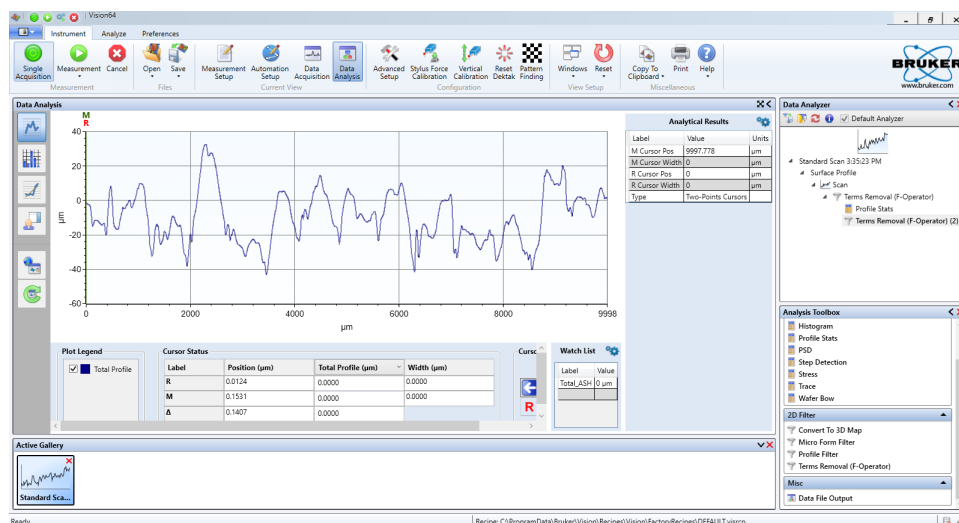
Figure 4.7.   profile of 10mm scan

Table 4.2. Calculated surface roughness for the DOE

Sample	Left (μm)	Center (μm)	Right (μm)	Average (μm)
1	20.31	18.94	27.22	22.16
2	17.39	23.2	14.13	18.24
3	22.34	17.39	11.56	17.1
4	17.61	13.07	16	15.56
5	14.12	15.84	11.68	13.88
6	14.44	18.25	17.98	16.89
7	13.3	16.29	16.26	15.28
8	13.52	24.39	14.75	17.55
9	15.85	16.11	14.44	15.47
10	14.28	18.89	15.88	16.35
11	10.79	15.78	14.99	13.85
12	20.98	19.71	18.36	19.68
13	10.6	21.04	9.83	13.82
14	11.26	14.82	11.68	12.59
15	16.05	12.87	14.5	14.47
16	11.18	13.2	9.49	11.29
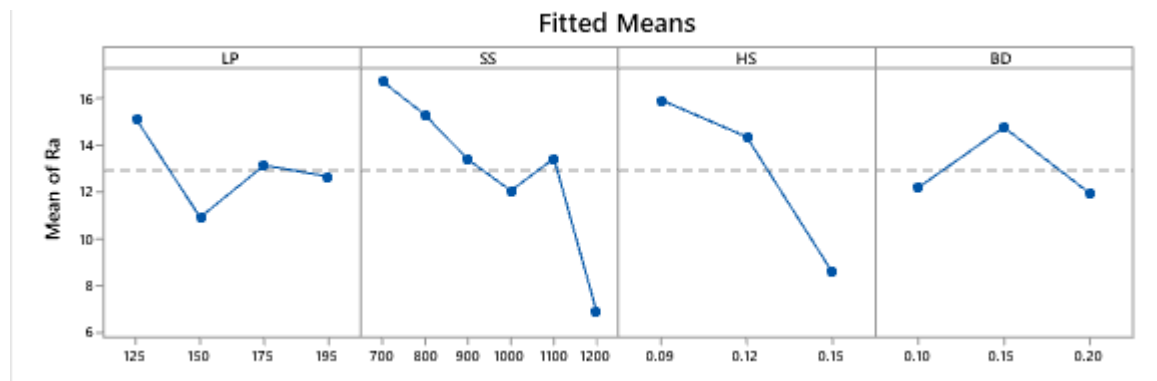
Figure 4.8. Main effects plot for R_a

Table 4.2 presents the average roughness values of all the sets of DOE. For surface roughness, equation 3.4 is used to calculate the S/N ratio and is represented in figure

4.8. From figure 4.8, it can be clearly seen that decreasing the SS or HS reduces the R_a.Also, from table 3.10 P-value, it should be noted that SS and LP followed by BD and HS show progressive effect on the surface roughness.

Table 4.3. ANOVA for R_a vs LP, SS, HS BD

Source	DF	Seq SS	Adj SS	Adj MS	F-value	P-value
LP	3	53.94	18.65	6.215	1.65	0.346
SS	5	21.39	28.31	5.663	1.50	0.392
HS	2	11.83	15.60	7.802	2.07	0.272
BD	2	13.38	13.38	6.690	1.77	0.310
Error	3	11.31	11.31	3.770		
Total	15	111.84				

4.2.2 Hardness

Three readings from corners and center are taken and the average is calculated as the final hardness of the part. Table 4.4 shows the calculated hardness values for the DOE.

Table 4.4. S/N ratio for samples with different hardness

Sample	Hardness, HRB	S/N ratio	Sample	Hardness, HRB	S/N ratio
1	86.6	38.75	9	91	39.18
2	94.8	39.54	10	91.5	39.23
3	93.23	39.39	11	88.57	38.95
4	93.67	39.43	12	92.23	39.3
5	89.13	39.00	13	89.47	39.03
6	89.9	39.07	14	89.5	39.04
7	89.6	39.05	15	92.87	39.36
8	93.03	39.37	16	93.6	39.42

From the HRB and S/N ratio in table 4.4, it is evident that hardness value is almost constant with a variation of ± 5. This proves that, the parameters changes within the maximum densification range doesn't affect the hardness value irrespective of the individual parameter selection setting as long as the VED falls in the optimized range.

4.2.3 Charpy impact test

Impact test is conducted on the 16 samples from phase II. Table 4.5 shows the results obtained. ANOVA is conducted to calculate the P-value which illustrates the impact/importance of each process parameter on the energy absorbed. Table 4.6 shows the ANOVA results. From the results, it is evident from P-value that SS has the major influence on the impact strength followed by HS, LP and BD. With increase in SS fixing the other parameters constant, there is a drop in impact strength of the samples (refer table 4.5). Similarly, with increase in LP, fixing other parameters constant, there is an increase in impact strength of the samples. This might be the result of better melting/sintering of the powder material leading to formation of stable meltpool.

Table 4.5. Impact test results for 16 samples from phase II

Sample	Impact strength (J)	sample	Impact strength (J)
1	148	9	137.2
2	144	10	143.8
3	127.5	11	109.5
4	136.5	12	120.5
5	150.2	13	126.2
6	124	14	140
7	129.6	15	134.2
8	134.5	16	132.2

Table 4.6.   ANOVA for impact strength vs LP, SS, HS & BD

Source	DF	Adj SS	Adj MS	F-value	P-value
LP	3	78.49	26.262	14.32	0.028
SS	5	40.70	8.140	4.46	0.124
HS	2	50.12	25.062	13.72	0.031
BD	2	122.40	61.202	33.50	0.009
Error	3	5.48	1.827		
Total	15	1713.12			

5. PREDICTIVE MODELLING: A NEURAL NETWORK APPROACH

5.1 Introduction

In the PBF process, with different parameters having a strong influence on the quality characteristics of the fabricated part, it is complicated to establish simple relations between the non-linear correlation of process parameters and quality properties. In chapter 3, the influence of each parameter on the tested quality properties is presented but based on those estimations, a complete process cannot be predicted for any required part. For instance, to reduce the fabrication time, SS will be increased; but with high SS, melt pool instability occurs leading to the formation of in-process defects. Each individual part will have a different set of process parameters which can achieve a better quality of the part. Based on the application, the requirement for certain quality property will be required. So, a good scenario to solve this issue is to develop a system which can auto select the process parameters based on the requirements of the manufacturer/end user. There are two main methods for modelling a manufacturing process. First, a physics-based and second, data-driven modelling. The physics-based modelling technique analyzes a manufacturing process from a physical point of view. However, this traditional analytical modelling method is not always suitable to model some modern complex manufacturing processes, such as AM, due to the number of process variables and the non-linear complex nature of the process.

Another modelling method is empirical modelling, which employs experimental data and statistical theory [66]. Many applications in manufacturing engineering successfully implemented machine learning (ML) and ANN methodology as a good empirical modelling method. In this research, an empirical model is developed in three ways i.e. using SVR and random forest methods in ML and ANN. Detailed

explanation about the approaches, results and the best approach to be used in future according to the error rates, loss function, uncertainty and stability are discussed in the following sections.

5.2 Machine learning

Machine learning is a branch of artificial intelligence. It is a method of data analysis which automates the building a model analytically based on the data. It reads the data, analyzes the patterns by assigning some random weights to come up with a certain weight for forming the relation analytically with minimal human interaction. The major advantages of ML are the capability of data preparation, analysis, scalability and automation of the iterative process. Apart from the data, no custom coding is required as it learns from the data and builds an own logic and function. Figure 5.1 shows the different classifications and algorithms employed.In this work, we are using support vector regression (SVR) and random forest regression techniques for training a function.

5.2.1 Support vector regression (SVR)

In SVR, hyperplane with maximum margin is identified in a way that a maximum number of data points fall within that boundaries. Instead of eliminating/reducing the error rate as carried out in simple linear regression, we try to adjust the error within a certain threshold. Our objective in SVR is to basically consider the points that are within the margin. The best fit line is the hyperplane that has the greatest number of points within the boundaries. The 16 sets of data are divided into two parts, 13 sets for training and 3 sets for testing. Heatmap is calculated for the input data to investigate any possible correlation between the inputs. If there is any correlation above ±0.5, then one of those parameters can be eliminated from the training set as it has a correlation with another input level and doing so increases the efficiency of the predictions. The top half above the diagonal can be neglected as
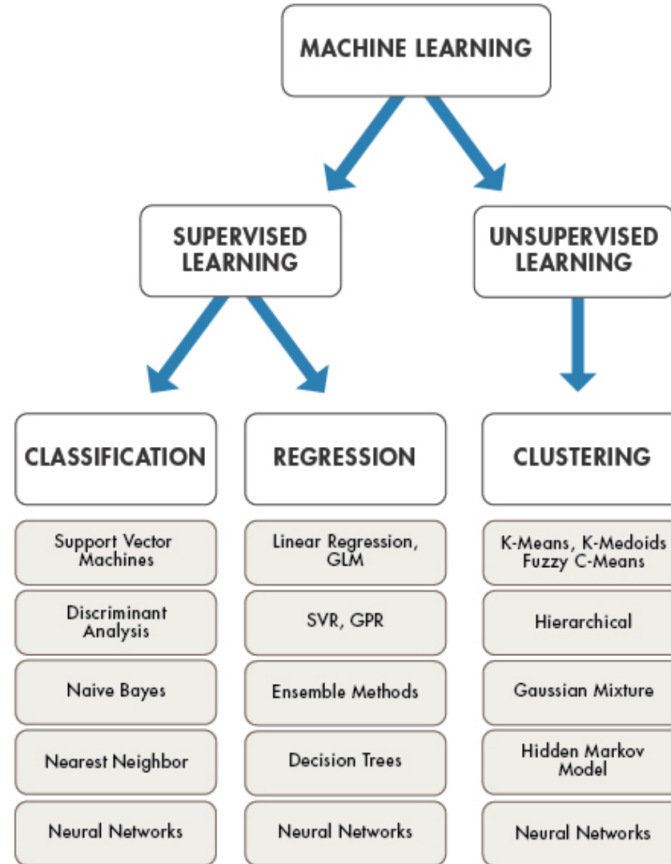
Figure 5.1. Machine learning: classification and algorithms

it is the replica of the bottom half. Also, the diagonal is neglected as it represents the correlation between the same inputs. Figure 5.2 shows the heat map calculated for the 13 sets of data. The R^2 value of 0.4511 is obtained. After training the data, testing is conducted on the 3 sets of data. Table 5.1 shows the predicted value and error percentage for each set for surface roughness prediction. An error percentage between 12.92 and 34.47 is obtained from the predicted values with a mean error of 20.18%. More data need to be incorporated into the SVR model for obtaining a constant error. Similarly, for every output, a model is developed and finally all model functions are put together into a single program which will result in achieving the input parameters according to the quality requirements.
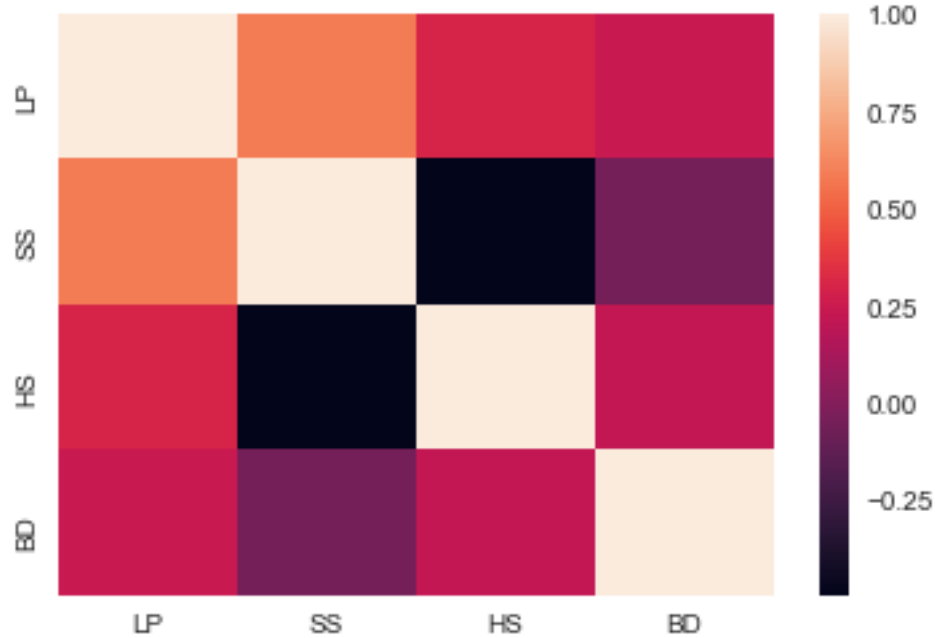
Figure 5.2. Heatmap for the training data

Table 5.1. SVR method: actual vs predicted value for surface roughness

Test data	Actual $R_a value$	Predicted $R_a value$	Error %
175,800,0.12,0.1	15.28	17.255	12.92
195,700,0.15,0.15	13.85	15.67	13.14
195,1000,0.09,0.1	12.59	16.93	34.47

5.2.2 Random forest regression

Random forest technique is one of the supervised learning model which can be used for both classification and regression model training. The major disadvantage with other models like SVR and NN is uncertainty. The uncertainty of a data set will result in increasing error in the predictions and with other techniques, as the data is used together, there is no way to reduce uncertainty in the predictions. But with random forest technique, the data is divided into groups of data called as trees or

bagging (figure 5.3) and the model runs in each tree and finally the average or the best value is given as prediction. In this way, if there is an error in one of the data set which leads to huge error in the prediction, the final predicted output will not have a major effect because of the average of the trees used. The only possibility of wrong prediction is if more than half of data is misleading.

Figure 5.3. Random forest model

Out of 16 data set, 12 are assigned as training data and 4 as testing data. Three trees are used dividing the training data into three random group. Trees number is estimated by running the model with 2 to 6 trees and out of all the values, 3 trees gave the minimum error with better R^2 value. Table 5.2 shows the predictions vs actual

data. The predictions shown in table 5.2 show that the error was between 23-27%. With just 12 set of training data, an accuracy 23-27% is obtained. Incorporating more data into the model will reduce the error to minimum.
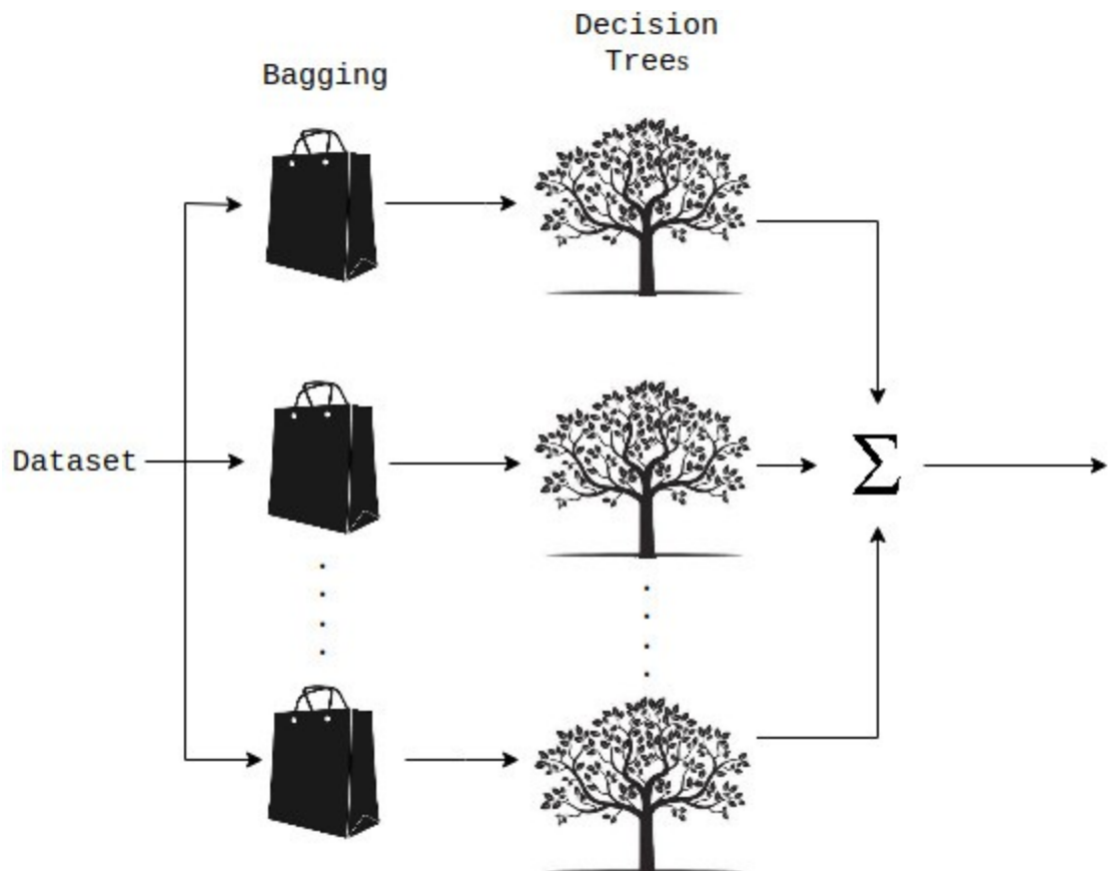
Table 5.2. Random forest method: actual vs predicted value for surface roughness

Test data	Actual $R_a value$	Predicted $R_a value$	Error %
175,800,0.12,0.1	15.28	19.35	26.64
195,700,0.15,0.15	13.85	17.122	23.624
195,1000,0.09,0.1	12.59	15.57	23.67

5.3 Neural network

With the non-linear data of process parameters and quality characteristics in AM processes, the ML technique which learns a pattern or forms a function for all the data is not realistic. For this kind of non-linear data, a system needs to be developed which can self-learn and update the knowledge base after each experiment to come up with better weight factors or functions. The artificial neural network which resembles the structure of the human brain having highly interconnected nodes between input and output is a more generalized approach. Scholars have been using ANN for developing time models and quality models. In this work, a multi-layer feed forward back propagating neural network is developed with LP, SS, HS and BD as features/inputs and UTS, impact strength, fabrication time and SR as labels/outputs (figure 5.4). Here, inputs or process parameters are called features and outputs are called labels. The NN network consists of three parts namely input layer (process parameters), hidden layer and output layer (ultimate properties). The hidden layer connects the input and output layers. In this work, one hidden layer with three nodes is used and to simulate the network, python programming is be used. The results and data acquired from the framework will be initially used for creating a knowledge

base. The NN system uses the acquired experimental data for training a function which acts as a learning engine. The weights will be calculated and adjusted by BP which gradually brings the output closer to the required output. Out of 16 sets of data, we divided the data as 12 sets of experiments for training data and 4 for testing data. The BP algorithm is employed for developing a knowledge learning module in the optimization model which requires the following stages

Figure 5.4. The schematic ANN architecture of this research
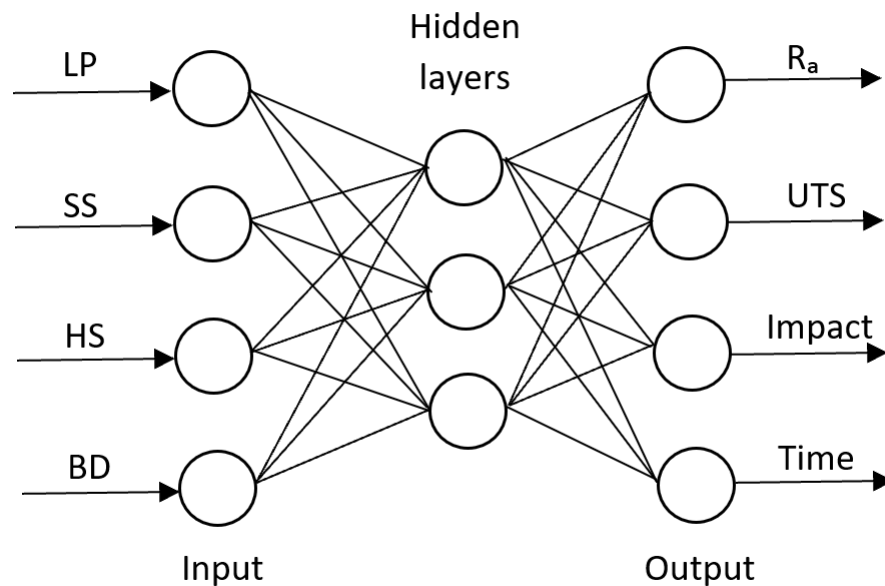
1. Importing the inputs and outputs as a matrix.

2. Set random weights and multiply with input.

3. Applying the activation function.

4. Calculate and return the output. Error is calculated by considering the difference between actual and predicted data.

5. Weights will be adjusted by the program. process is continued till the weight factor reaches to the best value.

However, for more accurate results and efficient prediction of the trained network, more data will have to be incorporated to make the network more complex. In python, for developing an ANN, the sigmoid function is used (figure 5.5). As sigmoid function varies from 0 to 1, the input and output are scaled down to between o and 1 by an activation function. Activation function introduces non-linearity and scales down the values to 0 and 1 which makes the training of weights for the function easier. Once the network is forwarded from input to output by assigning some random value, the learning of the network by back propagation (BP). BP uses a loss function for calculating the error between the calculated value and the target value. The loss function is calculated by the mean squared loss sum showed in equation 4.1

Sigmoid

$$f(x) = \frac{1}{1+e^{-\beta x}}$$
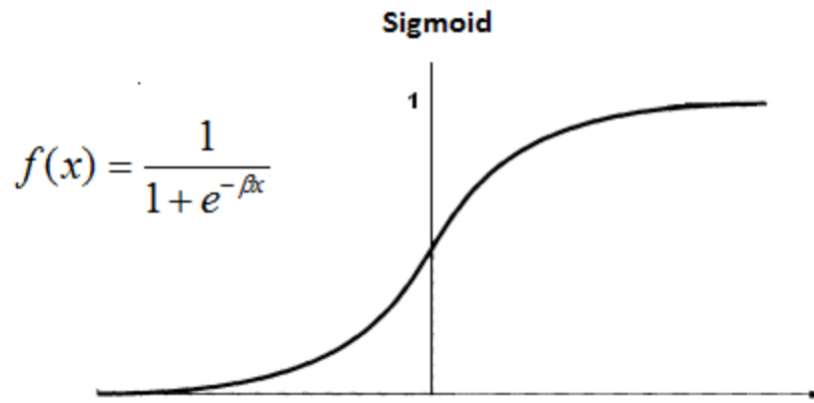
Figure 5.5. Sigmoid function

$$Loss = \sum (0.5)(o-y)^2 \qquad (5.1)$$

where o is the output predicted and y is the actual output. The network is trained individually for each output and the networks for all quality properties will be run together in one program at the end of developing a network for each property. A network is developed for predicting the surface roughness values. after training the network, it is tested for predicting the R_a for training data. Figure 5.6 and 5.7 shows

the actual and predicted values for training data, scatter plot with best fit and table 5.3 shows the error percentage. From table 5.3, the mean error rate of 10.236% is obtained with a loss function of 0.0002946. With lower loss function ideal being 0, the weights will be adjusted to the best values which gives predictions accurately with minimum error between actual and predicted data. Table 5.4 shows the predictions and error rate for test data. More data need to be incorporated for obtaining accurate predictions outside the working range of process parameters.

```
Input:
[[0.64102564 0.58333333 0.75       0.5       ]
 [0.64102564 0.66666667 0.75       1.        ]
 [0.76923077 0.66666667 0.75       1.        ]
 [0.76923077 0.75       0.75       0.5       ]
 [0.8974359  0.58333333 1.         1.        ]
 [0.8974359  0.75       0.75       0.75      ]
 [0.8974359  0.83333333 0.75       1.        ]
 [0.8974359  0.91666667 0.75       0.5       ]
 [1.         0.66666667 1.         0.75      ]
 [1.         0.75       1.         1.        ]
 [1.         0.91666667 0.75       1.        ]
 [1.         1.         0.75       0.75      ]]
Actual Output:
[[0.2216]
 [0.1824]
 [0.1556]
 [0.1388]
 [0.1689]
 [0.1755]
 [0.1547]
 [0.1635]
 [0.1968]
 [0.1382]
 [0.1447]
 [0.1129]]
Predicted Output:
[[0.20999464]
 [0.16876091]
 [0.16806588]
 [0.1743036 ]
 [0.18194029]
 [0.16326568]
 [0.14367527]
 [0.14820132]
 [0.17638114]
 [0.15392108]
 [0.13400007]
 [0.13145707]]
Loss:
0.0002945725155039534
```

Figure 5.6. predictions of the network

From the results of SVR, random forest and FF BP neural network, SVR method is not the ideal method for developing a predictive function as the error rate is not constant and is varying in a range (Table 5.1). Random forest method with three trees lead to almost stable error rate and with limited number of experiments, the

Table 5.3. Training data: Actual vs predicted data with percentage error

Training data	Actual $R_a value$/100	Predicted $R_a value$	Error %
125,700,0.09,0.1	0.2216	0.21	5.2346
125 ,800 ,0.09 ,0.2	0.1824	0.169	7.3465
150 ,800 ,0.09 ,0.2	0.1556	0.168	7.9691
150 ,900, 0.09, 0.1	0.1388	0.1743	25.5764
175 ,700 ,0.12 ,0.2	0.1689	0.1819	7.6966
175,900,0.09,0.15	0.1755	0.1633	6.9515
175,1000,0.09,0.2	0.1547	0.1437	7.1105
175, 1100, 0.09, 0.1	0.1635	0.1482	9.3578
195 ,800 ,0.12 ,0.15	0.1968	0.1764	10.3658
195 ,900, 0.12, 0.2	0.1382	0.1539	11.3603
195, 1100,0.09,0.2	0.1447	0.134	7.3946
195,1200,0.09,0.15	0.1129	0.1315	16.4748

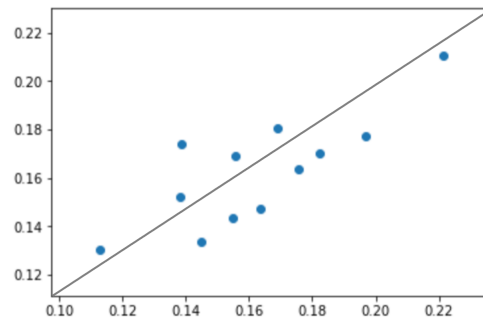Figure 5.7. Training data scatter plot with best fit line

error rate achieved is significantly better. Similarly FF BP NN trained a network with loss rate of 0.0002945 which is promising for making the network stable with more experiments. Hence, in future, both random forest and FF BP NN will be used to study the uncertainty finally developing a network with minimum error without overfitting.

Table 5.4. Testing data: Actual vs predicted data with percentage error

Test data	Actual $R_a value$/100	Predicted $R_a value$	Error %
150,700,0.12,0.15	0.171	0.1892	10.6433
175,800,0.12,0.1	0.1528	0.1832	19.8953
195,700,0.15,0.15	0.1385	0.1773	20.8159
195,1000,0.09,0.1	0.1259	0.15311	21.6124

By integrating this system with an online monitoring and control (OMC) system, nearly flawless parts with the desired ultimate qualities (the long-term objective) can be fabricated. Plentiful research nowadays has focused on the development of OMC systems [67-72] to avoid/diminish the defects and abnormalities generated during the fabrication process [24, 25, 37, 73-75]. Monitoring and control of the thermal specifications and thermal evolution of any inherently thermal AM process has been recognized as a crucial step towards improving the microstructure and ultimate mechanical properties of a fabricated part [76-78]. Nowadays, most vendors try to handle the frequent thermal anomalies of the fabricated parts such as distortion by designing some temporary support structures. These supports facilitate the conduction during the fabrication process and strengthen the structure. Designing the topology-optimized support structures reduces the fabrication time and material [79] however the fabricated parts still need significant work for post-processing. Optimization of process parameters by using an ANN model in this project integrated with an OMC system can considerably improve the mechanical properties and surface quality of fabricated parts, increase the repeatability, reduce fabrication time, and significantly decrease the need for the post-processing operations.

6. CONCLUSIONS AND FUTURE WORKS

6.1   Conclusions

In this work, addressing the mentioned gaps and challenges existing in PBF process, a two-phase framework is proposed for optimizing the process parameters thereby achieving maximum density and better ultimate properties of the fabricated part and a predictive function is developed using different approaches for intelligent prediction of mechanical and quality properties for a given set of process parameters.

First, a mathematical model is developed to estimate the range of VED to be studied in phase-I and obtained that the lower limit and upper limit of VED are 57.89 J/mm^3 and 137.5 J/mm^3. Within this obtained VED range from mathematical model, SA is conducted to realize the influence of LP, SS, HS, and LT on the heat input per unit volume i.e. VED. The results from SA clearly shows that SS has the major influence on the VED working range followed by LP and HS. In this work, SS316L material is used and LT is kept at machine constant value of 0.02 mm. Then two DOEs are conducted as part of two phases to study different process parameters and their significance on mechanical and quality properties of the fabricated part aiming to achieve different objectives in each phase.

In phase I, full factorial analysis is conducted within VED range obtained from mathematical model and by merely changing LP and SS keeping the other values at machine constants. LP was varied between 100 W to 175 W and SS was varied between 700 mm/s to 1000 mm/s. 16 cubic samples with the dimensions 10 mm x 10 mm x 5 mm were fabricated. The samples were cut parallel and perpendicular to the build direction using WEDM process and porosity and microstructure were studied using SEM. The results prominently showed formation of gas pores and LOF pores at the high and low VED ranges leading to formation maximum porosity. Whereas, the

porosity reduced steeply in the range between 90 J/mm^3 and 105 J/mm^3. Densities between 95.52% and 99.31% with a maximum of 99.31% is achieved. From the results, the optimum range obtained for VED is 90 J/mm^3 and 105 J/mm^3 with a maximum density of 99.31%. Also, the results suggest the optimized range between 150 W to 200 W for the laser power and 800 mm/s to 1000 mm/s for scan speed to obtain the maximum densification. These results of optimum values for achieving maximum density are carried forward to phase II for further understanding of process parameters on ultimate quality of the fabricated part.

In phase II, the optimum range obtained from phase I is employed and the influence of LP, SS, HS and BD on surface roughness and mechanical properties were studied with objective of correlating process parameters with quality properties of the fabricated part. Taguchi method is used for DOE with 16 sets of experiments. For each experiment, 3 samples were fabricated according to ASTM E8, ASTM E23, and ASTM E18 standards. S/N ratio and ANOVA is conducted to obtain the F-value and P-value. Rockwell hardness is used for hardness measurement using HRB tester with a force of 150 KgF. Three readings were taken on the sample and averaged to obtain the hardness value. From the hardness results obtained, for all the samples the hardness values are $\pm$ 4 from 90. This proves that irrespective of the combination of parameters or values of each parameter within the optimum range of VED, the hardness values will almost be the same with a minor variation. We can imply that; the hardness values are correlated with porosity. The lower the porosity, the better the hardness of the fabricated part.

For surface roughness, Bruker DektakXT system with a stylus of 2μm radius, force of 5mg, speed of 600 μm/s and time duration of 25 seconds is used. Three measurements of 10 mm length are scanned and averaged for obtaining the R_a value reducing the uncertainty in the results. From the results of S/N and ANOVA, it can be clearly noticed that decreasing the SS or HS reduces the R_a. Also, from P-value, it should be noted that SS and LP followed by BD and HS show progressive effect on the surface roughness. From the results from phase II, the correlation between

process parameters and quality properties is obtained which is finally used to develop a network for intelligent predictive modelling of process parameters in PBF process using different approaches in ML and ANN.

Finally, employing the results obtained from phase II, using ML and ANN techniques an algorithm and network is developed for predictive modelling. In ML, SVR method is used for training an algorithm for surface roughness prediction with given set of process parameters. Primarily, heatmap is generated to realize the correlation between inputs and from the results, it is observed that all inputs are independent without any linear dependence. After training the algorithm with 13 sets of data, 3 sets of data are used for validation and from the validation, an error percentage between 12.92 and 34.47 % is achieved.

A feed forward back propogating neural network is developed with three layers i.e. input layer, one hidden layer with 3 nodes, and output layer. Sigmoid function is used and the input, output values are scaled down to values between 0 and 1. The data is divided into 12 sets of training data and 4 sets of test data. After training the function, the network is validated by test data. From the results, the mean error obtained is 10.236% with a loss function of 0.0002945. With just 12 sets of data, the network is trained for predictive modelling with a minimum error. For further development of the network and to make the loss function ideal, more data needs to be incorporated.

In summary, the proposed framework proves its capability to study the influence of the process parameters on the quality properties of the fabricated part providing better insight into the complex nature of working with multiple process parameters. Also, employing this framework ensures maximum density parts with better mechanical properties. With the predictive model developed in the framework, the biggest challenge of uncertainty in the quality properties of fabricated part is addressed leading to stability of the process.

6.2   Future works

With the prominent results obtained from the framework, more research has to be conducted to complete the framework and to make it standardized approach which include

- Phase-II will have to be completed by conducting the remaining tests.

- A FFBP NN for all inputs and outputs will have to be developed.

- More data will be included for making the network stable with a minimum error.

- A GUI will be developed with ability to make it more user-friendly.

- Different samples have to be tested and included in the network for making the framework and the modelling of the process complete.

- Finally, the network will have to be calibrated on different machine to realize the scope and efficiency.

REFERENCES

REFERENCES

[1] Arasu, I., et al., Optimization of surface roughness in selective laser sintered stainless steel parts. Vol. 6. 2993-2999. 2014.

[2] Yasa, E., et al., A Study on the Stair Stepping Effect in Direct Metal Laser Sintering of a Nickel-based Superalloy. Procedia CIRP. 45: p. 175-178. 2016.

[3] Hanzl, P., et al., The Influence of Processing Parameters on the Mechanical Properties of SLM Parts. Vol. 100. 2015.

[4] Dingal, S., et al., The application of Taguchis method in the experimental investigation of the laser sintering process. Vol. 38. 904-914. 2008.

[5] Hardik Varia, B.G., A Review on Effect of Process Parameters on Surface Quality and Properties of Parts Realized by Selective Laser Sintering Process. International Journal on Recent and Innovation Trends in Computing and Communication (IJRITCC), p. 45-51.2017.

[6] Custompart.net: 'Direct Metal Laser Sintering'. [cited 2018 June 25]; Available from: http://www.custompartnet.com/wu/direct-metal-laser-sintering.

[7] Verma, A., P.S. Tyagi, and K. Yang, Modeling and optimization of direct metal laser sintering process. Vol. 77. 2014.

[8] Gu, D. and Y. Shen, Processing conditions and microstructural features of porous 316L stainless steel components by DMLS. Applied Surface Science. 255(5, Part 1): p. 1880-1887. 2008.

[9] Mohammadi, M. and H. Asgari, Achieving low surface roughness AlSi10Mg200C parts using direct metal laser sintering. Additive Manufacturing. 20: p. 23-32. 2018.

[10] Patil, N.S., E. Malekipour, and H. El-Mounayri, Development of a Cone CVT by SDPD and Topology Optimization. SAE Technical Paper. 2019.

[11] Calignano, F., et al., Influence of process parameters on surface roughness of aluminum parts produced by DMLS. The International Journal of Advanced Manufacturing Technology. 67(9): p. 2743-2751. 2013.

[12] DMLS.com. DMLS applications. [cited 2018 10/01]; Available from: http://dmls.com/dmls-applications.

[13] Stratasys. Direct metal laser sintering materials. [cited 2018 10/01]; Available from: https://www.stratasysdirect.com/materials/direct-metal-laser-sintering.

[14] Maleki Pour, E. and S.J.I.J.o.a.e. Golabi, Design of continuously variable transmission (CVT) with metal pushing belt and variable pulleys. 4(2): p. 699-717. 2014.

[15] Pour, E.M., S.i.J.I.J.o.A.o.I.i.E. Golabi, and Management, Examining the Effects of Continuously Variable Transmission (CVT) and a new mechanism of planetary gearbox of CVT on Car Acceleration and Fuel Consumption. 2014.

[16] Gong, H., et al., Defect Morphology of Ti-6Al-4V Parts Fabricated by Selective Laser Melting and Electron Beam Melting. 2013.

[17] Fox, J.C., S.P. Moylan, and B.M. Lane, Effect of Process Parameters on the Surface Roughness of Overhanging Structures in Laser Powder Bed Fusion Additive Manufacturing. Procedia CIRP. 45: p. 131-134. 2016.

[18] Kumar, N., H. Kumar, and J.S. Khurmi, Experimental Investigation of Process Parameters for Rapid Prototyping Technique (Selective Laser Sintering) to Enhance the Part Quality of Prototype by Taguchi Method. Procedia Technology. 23: p. 352-360. 2016.

[19] Delgado, J., J. Ciurana, and C.A. Rodrguez, Influence of process parameters on part quality and mechanical properties for DMLS and SLM with iron-based materials. The International Journal of Advanced Manufacturing Technology. 60(5): p. 601-610. 2012.

[20] Konen, R., et al., Long Fatigue Crack Growth in Ti6Al4V Produced by Direct Metal Laser Sintering. Vol. 160. 2016. 69-76.

[21] Pal, S., et al., The Effect of Post-processing and Machining Process Parameters on Properties of Stainless Steel PH1 Product Produced by Direct Metal Laser Sintering. Vol. 149. 359-365. 2016.

[22] Yadroitsev, I., P. Bertrand, and I. Smurov, Parametric analysis of the selective laser melting process. Applied Surface Science. 253(19): p. 8064-8069. 2007.

[23] Spears, T.G. and S.A. Gold, In-process sensing in selective laser melting (SLM) additive manufacturing. Integrating Materials and Manufacturing Innovation. 5(1): p. 2. 2016.

[24] Malekipour, E. and H. El-Mounayri, Defects, process parameters and signatures for online monitoring and control in powder-based additive manufacturing, in Mechanics of Additive and Advanced Manufacturing, Volume 9. Springer. p. 83-90. 2018.

[25] Malekipour, E. and H. El-Mounayri, Common defects and contributing parameters in powder bed fusion AM process and their classification for online monitoring and control: a review. The International Journal of Advanced Manufacturing Technology. 95(1): p. 527-550. 2018.

[26] Van Elsen, M., Complexity of selective laser melting: a new optimisation approach. Diss Katholieke Universiteit Leuven. Retrieved July 2, 2019, from http://citeseerx.ist.psu.edu.

[27] Ruban, W., et al., Effective process parameters in selective laser sintering. International Journal of Rapid Manufacturing. 4(2-4): p. 148-164. 2014.

[28] Ehsan Malekipour, H.E.-M., Mohammad Al Hasan, Eric J. Faierson, A Vision toward Layer-wise Intelligent Monitoring and Control of Scan Strategy in Powder-bed Fusion Process. TechConnect Briefs. p. 127-130. 2019.

[29] Marrey, M., et al., A framework for optimizing process Parameters in powder bed fusion (PBF) process using artificial neural network (ANN). Procedia Manufacturing. 34: p. 505-515. 2019.

[30] Dilberoglu, U.M., et al., The role of additive manufacturing in the era of industry 4.0. 11: p. 545-554. 2017.

[31] DebRoy, T., et al., Additive manufacturing of metallic components Process, structure and properties. Progress in Materials Science. 92: p. 112-224. 2018.

[32] O'Neill, W., et al., Investigation on Multi-Layer Direct Metal Laser Sintering of 316L Stainless Steel Powder Beds. CIRP Annals. 48(1): p. 151-154. 1999.

[33] Liverani, E., et al., Effect of selective laser melting (SLM) process parameters on microstructure and mechanical properties of 316L austenitic stainless steel. 249: p. 255-263. 2017.

[34] Yadroitsev, I., et al., Factor analysis of selective laser melting process parameters and geometrical characteristics of synthesized single tracks. 18(3): p. 201-208. 2012.

[35] Sun, Z., et al., Selective laser melting of stainless steel 316L with low porosity and high build rates. 104: p. 197-204. 2016.

[36] Ahmadi, A., et al., Effect of manufacturing parameters on mechanical properties of 316L stainless steel parts fabricated by selective laser melting: A computational framework. 112: p. 328-338. 2016.

[37] Taheri, H., et al., Powder-based additive manufacturinga review of types of defects, generation mechanisms, detection, property evaluation and metrology. 1(2): p. 172. 2017.

[38] Kamath, C., et al., Density of additively-manufactured, 316L SS parts using laser powder-bed fusion at powers up to 400 W. 74(1-4): p. 65-78. 2014.

[39] Gu, D., Y.J.M. Shen, and Design, Balling phenomena in direct laser sintering of stainless steel powder: Metallurgical mechanisms and control methods. 30(8): p. 2903-2910. 2009.

[40] Gu, H., et al. Influences of energy density on porosity and microstructure of selective laser melted 17-4PH stainless steel. in 2013 Solid Freeform Fabrication Symposium. 2013.

[41] Guan, K., et al., Effects of processing parameters on tensile properties of selective laser melted 304 stainless steel. Vol. 50. 581586. 2013.

[42] Vandenbroucke, B. and J.-P.J.R.P.J. Kruth, Selective laser melting of biocompatible metals for rapid manufacturing of medical parts. 13(4): p. 196-203. 2007.

[43] Abele, E., et al., Selective laser melting for manufacturing of thin-walled porous elements. 215: p. 114-122. 2015.

[44] Shen, N. and K. Chou. Thermal modeling of electron beam additive manufacturing process: powder sintering effects. in ASME 2012 International Manufacturing Science and Engineering Conference collocated with the 40th North American Manufacturing Research Conference and in participation with the International Conference on Tribology Materials and Processing. American Society of Mechanical Engineers. 2012.

[45] Bertoli, U.S., et al., On the limitations of volumetric energy density as a design parameter for selective laser melting. 113: p. 331-340. 2017.

[46] Barua, S., et al., Vision-based defect detection in laser metal deposition process. 20(1): p. 77-85. 2014.

[47] Meier, H. and C.J.M.u.W. Haberland, Experimental studies on selective laser melting of metallic parts. 39(9): p. 665-670. 2008.

[48] Liu, Q.C., et al. The effect of manufacturing defects on the fatigue behaviour of Ti-6Al-4V specimens fabricated using selective laser melting. Advanced Materials Research. Trans Tech Publ. 2014.

[49] Louvis, E., P. Fox, and C.J.J.J.o.M.P.T. Sutcliffe, Selective laser melting of aluminium components. 211(2): p. 275-284. 2011.

[50] Lee, Y. and D.J.T.I.J.o.A.M.T. Farson, Surface tension-powered build dimension control in laser additive manufacturing process. 85(5-8): p. 1035-1044. 2016.

[51] Bassoli, E., et al., Development of Laser-Based Powder Bed Fusion Process Parameters and Scanning Strategy for New Metal Alloy Grades: A Holistic Method Formulation. 11(12): p. 2356. 2018.

[52] Cheng, B. and K. Chou. Melt pool evolution study in selective laser melting. in 26th Annual International Solid Freeform Fabrication Symposium-An Additive Manufacturing Conference, Austin, TX, USA. 2015.

[53] Hamby, D.M., A review of techniques for parameter sensitivity analysis of environmental models. Environmental Monitoring and Assessment. 32(2): p. 135-154. 1994.

[54] Read, N., et al., Selective laser melting of AlSi10Mg alloy: Process optimisation and mechanical properties development. Vol. 65. 417-424. 2015.

[55] Sufiiarov, V.S., et al., The Effect of Layer Thickness at Selective Laser Melting. Procedia Engineering. 174: p. 126-134. 2017.

[56] Zhao, X., et al., Numerical modeling of the thermal behavior and residual stress in the direct metal laser sintering process of titanium alloy products. Additive Manufacturing. 14: p. 126-136. 2017.

[57] C. Hofland, E., I. Baran, and D. Wismeijer, Correlation of Process Parameters with Mechanical Properties of Laser Sintered PA12 Parts. Vol. 1-11. 2017.

[58] Thijs, L., et al., A study of the microstructural evolution during selective laser melting of Ti6Al4V. Acta Materialia. 58(9): p. 3303-3312. 2010.

[59] Pianosi, F., F. Sarrazin, and T. Wagener, A Matlab toolbox for Global Sensitivity Analysis. Environmental Modelling & Software. 70: p. 80-85. 2015.

[60] Gangireddy, S., et al., Microstructure and mechanical behavior of an additive manufactured (AM) WE43-Mg alloy. 26: p. 53-64. 2019.

[61] Palanivel, S., et al., Spatially dependent properties in a laser additive manufactured Ti6Al4V component. 654: p. 39-52. 2016.

[62] Wolff, S.J., et al., A framework to link localized cooling and properties of directed energy deposition (DED)-processed Ti-6Al-4V. 132: p. 106-117. 2017.

[63] Yan, F., W. Xiong, and E.J.M. Faierson, Grain structure control of additively manufactured metallic materials. 10(11): p. 1260. 2017.

[64] Cherry, J.A., et al., Investigation into the effect of process parameters on microstructural and physical properties of 316L stainless steel parts by selective laser melting. The International Journal of Advanced Manufacturing Technology. 76(5): p. 869-879. 2015.

[65] ASTM, Standard Test Methods for Tension Testing of Metallic Materials, in E8 / E8M - 13. ASTM International, West Conshohocken, PA. 2013.

[66] Chen, H., A process modelling and parameters optimization and recommendation system for binder jetting additive manufacturing process. McGill Library and Collection. Retrieved June 25, 2019, from http://digitool.library.mcgill.ca.

[67] Amini, M., Chang, S. A review of machine learning approaches for high dimensional process monitoring. In Proceedings of the Industrial and Systems Engineering Research Conference, Orlando, FL. 2018.

[68] Amini, M. and S. Chang, Process Monitoring of 3D Metal Printing in Industrial Scale. (51357): p. V001T01A035. 2018.

[69] Amini, M. and S.I. Chang, MLCPM: A process monitoring framework for 3D metal printing in industrial scale. Computers Industrial Engineering, 2018. 124: p. 322-330.

[70] Imani, F., Gaikwad, A., Montazeri, M., Rao, P., Yang, H., Reutzel, E. Layerwise in-process quality monitoring in laser powder bed fusion. In ASME 2018 13th International Manufacturing Science and Engineering Conference (pp. V001T01A038-V001T01A038). American Society of Mechanical Engineers. June, 2018.

[71] Yao, B., et al., Multifractal Analysis of Image Profiles for the Characterization and Detection of Defects in Additive Manufacturing. Journal of Manufacturing Science and Engineering. 140(3): p. 031014-031014-13. 2018.

[72] Imani, F., et al., Process Mapping and In-Process Monitoring of Porosity in Laser Powder Bed Fusion Using Layerwise Optical Imaging. Journal of Manufacturing Science and Engineering. 140(10): p. 101009-101009-14. 2018.

[73] Montazeri, M., et al., In-Process Monitoring of Material Cross-Contamination Defects in Laser Powder Bed Fusion. Journal of Manufacturing Science and Engineering. 140(11): p. 111001-111001-19. 2018.

[74] Sedaghati, A. and H. Bouzary, A study on the effect of cooling on microstructure and mechanical properties of friction stir-welded AA5086 aluminum butt and lap joints. Proceedings of the Institution of Mechanical Engineers, Part L: Journal of Materials: Design and Applications. p. 1464420717726562. 2017.

[75] Igbelina, C., The Synergistic Integration of Mass Customization, Parametric Design and Additive Manufacturing: A Case of Personalized Footwear. (Doctoral dissertation, The University of Texas at San Antonio). 2018.

[76] Attoye, S., E. Malekipour, and H. El-Mounayri. Correlation Between Process Parameters and Mechanical Properties in Parts Printed by the Fused Deposition Modeling Process. in Mechanics of Additive and Advanced Manufacturing, Volume 8. Cham: Springer International Publishing. 2019.

[77] Malekipour, E., S. Attoye, and H. El-Mounayri, Investigation of Layer Based Thermal Behavior in Fused Deposition Modeling Process by Infrared Thermography. Procedia Manufacturing. 26: p. 1014-1022. 2018.

[78] Ebrahimpour, A., et al., Experimental Measurement and Numerical Simulation of Temperature Distribution and Thermal History During Friction Stir Welding of Pure Copper Joints. Journal of Mechatronics. 2(2): p. 113-118. 2014.

[79] Malekipour, E., A. Tovar, and H. El-Mounayri. Heat Conduction and Geometry Topology Optimization of Support Structure in Laser-Based Additive Manufacturing. in Mechanics of Additive and Advanced Manufacturing, Volume 9. Cham: Springer International Publishing. 2018.

[80] Nozar, M., Zetkov, I., Hronek, O. Searching for favourable powder bed fusion settings in sintering of maraging steel ms1. Annals of DAAAM Proceedings, 29. 2018.